

1 The sensitivity of primary productivity in
2 Disko Bay, a coastal Arctic ecosystem to
3 changes in freshwater discharge and sea
4 ice cover

5
6 Eva Friis Møller¹, Asbjørn Christensen², Janus Larsen¹, Kenneth D. Mankoff^{3,4,5}, Mads Hvid
7 Ribergaard⁶, Mikael Sejr¹, Philip Wallhead⁷, Marie Maar¹

8 ¹Department of Ecoscience, Aarhus University, 4000 Roskilde, Denmark

9 ²DTU Aqua, Technical University of Denmark, DK-2880 Kgs. Lyngby, Denmark

10 ³Department of Glaciology and Climate, Geological Survey of Denmark and Greenland, 1350
11 Copenhagen, Denmark

12 ⁴Business Integra, New York, NY, USA

13 ⁵NASA Goddard Institute for Space Studies, New York, NY, USA

14 ⁶Danish Meteorological Institute, 2100 Copenhagen, Denmark

15 ⁷Section for Oceanography, Norwegian Institute for Water Research (NIVA Vest), Bergen,
16 Norway

17 *Correspondence to:* Eva Friis Møller (efm@ecos.au.dk)

18 **Abstract.** The Greenland Ice Sheet is melting, and the rate of ice loss has increased 6-fold since
19 the 1980s. At the same time, the Arctic sea ice extent is decreasing. Melt water runoff and sea ice
20 reduction both influence light and nutrient availability in the coastal ocean with implications for
21 the timing, distribution and magnitude of phytoplankton production. However, the integrated
22 effect of both glacial and sea ice melt is highly variable in time and space, making it challenging
23 to quantify. In this study, we evaluate the relative importance of these processes for the primary
24 productivity of Disko Bay, West Greenland, one of the most important areas for biodiversity and
25 fisheries around Greenland. We use a high-resolution 3D coupled hydrodynamic-biogeochemical
26 model for 2004 to 2018 validated against *in situ* observations and remote sensing products. The
27 model estimated net primary production (NPP) varied between 90-147 gC m⁻² year⁻¹ during
28 2004-2018, a period with variable freshwater discharges and sea ice cover. NPP correlated
29 negatively with sea ice cover, and positively with freshwater discharge. Freshwater discharge
30 had a strong local effect within ~25 km of the source sustaining productive hot spot's during
31 summer. When considering the annual NPP at bay scale, sea ice cover was the most important
32 controlling factor. In scenarios with no sea ice in spring, the model predicted ~30% increase in
33 annual production compared to a situation with high sea ice cover. Our study indicates that
34 decreasing ice cover and more freshwater discharge can work synergistically and will likely
35 increase primary productivity of the coastal ocean around Greenland.

36 1 Introduction

37 The warming of the Arctic (Cohen et al., 2020) has a strong impact on the regional sea ice. Over
38 the past few decades, the sea ice melt season has lengthened (Stroeve et al., 2014), summer
39 extent has declined, and the ice is getting thinner (Meier et al., 2014). This has an immediate
40 effect on the primary producers of the ocean. The photosynthetic production is constrained by
41 the annual radiative cycle, and the sea ice reduces the availability of light and thereby the
42 development of the sea ice algae and the pelagic phytoplankton communities (Ardyna et al.,
43 2020). An extended open water period will affect the phenology of primary producers and
44 potentially lead to an earlier spring bloom (Ji et al., 2013; Leu et al., 2015), and may also
45 increase the potential for autumn blooms (Ardyna et al., 2014).

46 In the Arctic coastal ocean, there are additional impacts of a warming climate. As the freshwater
47 discharge increases due the melt of snow and ice on land and higher precipitation (Kjeldsen et
48 al., 2015; Mankoff et al., 2020a, 2021), the land-ocean coupling along the extensive Arctic
49 coastline is intensified (Hernes et al., 2021). The summer inflow of melt water has complex
50 biogeochemical impacts on the coastal ecosystem and combines with changes in sea ice cover to
51 affect the magnitude and phenology of marine primary production. In areas dominated by
52 glaciated catchments such as Greenland, the increase in melt water discharge has been
53 substantial and the rate of ice mass loss has increased sixfold since the 1980s (Mankoff et al.,
54 2020b; Mougnot et al., 2019).

55 The changes in sea ice cover and freshwater discharge will affect the marine primary production
56 through the complex interactions of changes in stratification, light and nutrient availability
57 (Arrigo and van Dijken, 2015; Hopwood et al., 2020). The individual processes are relatively
58 well described, but the interactions between them and the temporal and spatial importance under
59 different Arctic physical regimes are less well understood. A lower extent of sea ice cover may
60 also increase the wind-induced mixing of the water column and deepen or weaken the
61 stratification. Thereby, the potential for the phytoplankton to stay and grow in the illuminated
62 surface layer is reduced. At the same time, a higher mixing rate will increase the supply of new
63 nutrients from deeper layers to support production when light is not limiting (Tremblay and
64 Gagnon, 2009). Another mechanism affecting stratification is the freshening of the surface layer
65 due to ice melt from both sea ice and the ice sheet (von Appen et al., 2021; Holding et al., 2019).

66 If a glacier terminates in a deep fjord, the ice sheet melt is injected at depth causing more coastal
67 upwelling of nutrients (Hopwood et al., 2018; Meire et al., 2017)

68 The relative importance on productivity of sea ice versus glacier freshwater discharge depends
69 on the scale considered (Hopwood et al., 2019). Freshwater discharge from the ice sheet is more
70 important in the vicinity of the glacier (Hopwood et al., 2019; Meire et al., 2017), whereas the
71 sea ice dynamics are considered to be an important driver in the open ocean (Arrigo and van
72 Dijken, 2015; Massicotte et al., 2019; Meier et al., 2014). Most studies consider one or the other
73 separately (e.g. Hopwood et al., 2018; Vernet et al., 2021). However, in the coastal Arctic areas
74 at the mesoscale, i.e. 10-100 km, it can be expected that both sea ice and glacier freshwater
75 discharge and the interaction between them will influence the ecosystem and the pelagic primary
76 production (Hopwood et al., 2019). To resolve their relative impacts, we need to constrain their
77 impacts on both seasonal and spatial scales, which is a challenging task. A useful tool to achieve
78 such an integrated perspective is a high-resolution 3D coupled hydrodynamic-biogeochemical
79 model.

80 Disko Bay is located on the west coast of Greenland (Fig. 1) near the southern border of the
81 maximum annual Arctic sea ice extent, and is influenced by both sub-Arctic waters from
82 southwestern Greenland and Arctic waters within the Baffin Bay (Gladish et al., 2015; Rysgaard
83 et al., 2020). The bay has a pronounced seasonality in sea ice cover (Møller and Nielsen, 2020).
84 Over the last 40 years, there has been a pronounced decrease in sea ice cover, and also the year-
85 to-year variations have increased in the last decade (Fig 2, Hansen et al., 2006, the Greenland
86 Ecosystem monitoring program, <http://data.g-e-m.dk>). For the primary producers particularly the
87 decrease in sea ice cover during the time of the spring bloom in April is important (Møller and
88 Nielsen, 2020). In addition to the seasonal sea ice cover changes, the bay also experiences large
89 seasonal changes in freshwater input from the Greenland ice sheet, particularly during the
90 summer months (Fig. 2, 3). The large marine terminating glacier Sermeq Kujalleq (Jakobshavn
91 Isbræ) is found in the inner part of the bay. It is estimated that about 10% of the icebergs from
92 the Greenland ice sheet originate from this glacier (Mankoff et al., 2020a). Since the 1980s,
93 freshwater discharge from the Greenland Ice sheet to Disko Bay has almost doubled (Fig. 2,
94 (Mankoff et al., 2020b, 2020a). How these significant changes in sea ice dynamics and run-off

95 will impact the ecosystem in Disko Bay, one of the most important areas for biodiversity and
96 fisheries around Greenland (Christensen et al. 2012), is still not well understood.

97 In this study, we investigate the combined effect of changes in sea ice cover and the Greenland
98 ice sheet freshwater discharge on the phenology/seasonal timing and annual magnitude and
99 spatial distribution of the phytoplankton production in Disko Bay. We do so using a high-
100 resolution 3D coupled hydrodynamic-biogeochemical model validated against in situ
101 measurement of salinity, temperature, nutrients, phytoplankton, and zooplankton biomass. The
102 validated model allows us to estimate the impact of sea ice cover and freshwater discharge on
103 productivity with a higher temporal and spatial resolution than would be possible from
104 measurements alone.

105 2 Methods

106 2.1 Hydrodynamic model

107 The model was set up using the FlexSem model system (Larsen et al. 2020). FlexSem is an open
108 source modular framework for 3D unstructured marine modelling. The system contains modules
109 for hydrostatic and non-hydrostatic hydrodynamics, 3D pelagic and 3D benthic models, sediment
110 transport and agent-based models. The FlexSem source code and precompiled source code for
111 Windows (GNU General Public License) can be downloaded at
112 <https://marweb.bios.au.dk/Flexsem>. The specific code for the Disko set-up can be downloaded
113 on Zenodo.org (Larsen, 2022; Maar et al., 2022).

114 Bathymetry were obtained from the 150x150 m resolved IceBridge BedMachine Greenland,
115 Version 3 (<https://nsidc.org/data/IDBMG4> (Morlighem et al., 2017)) and interpolated to the
116 FlexSem computational mesh using linear interpolation. The 96,300 km² large computational
117 mesh for the Disko Bay area was constructed using the mesh generator JigSaw
118 (<https://github.com/dengwirda/jigsaw>) (Fig. 1). It consists of 6349 elements and 34 depth z-
119 layers with a total of 105678 computational cells. The horizontal resolution varies from 1.8 km
120 in the Disko Bay proper, 4.7 km in Strait of Vaigat and 16 km towards the semi-circular Baffin
121 Bay open boundary. In the deepest layers, the vertical resolution is 50 m, decreasing towards the
122 surface, where the top 5 layers are 3.5, 1.5, 2.0, 2.0 and 2.0 meters thick, respectively. The

123 surface layer thickness is flexible allowing changes in water level e.g., due to tidal elevations.
124 The model time step is 300 seconds and has been run for the period from 2004 to 2018.

125 **2.2 Biogeochemical model**

126 The biogeochemical model in the FlexSem framework was based on a modification of the
127 ERGOM model that originally was applied to the Baltic Sea and the North Sea (Maar et al.,
128 2011, 2016; Neumann, 2000) (Appendix A). In the Disko Bay version, 11 state variables
129 describe concentrations of four dissolved nutrients (NO_3 , NH_4 , PO_4 , SiO_2), two functional groups
130 of phytoplankton (diatoms, flagellates), micro- and mesozooplankton, detritus (NP), detritus-
131 silicon, and oxygen. Cyanobacteria present in the Baltic Sea version of the model are removed in
132 the current set-up, because cyanobacteria are of little importance in high-saline Arctic waters
133 (Lovejoy et al., 2007). Further, pelagic detrital silicon was added to better describe the cycling
134 and settling of Si in deep waters. The model currency is N using Redfield ratios to convert to P
135 and Si. Chlorophyll *a* (Chl *a*) was estimated as the sum of the two phytoplankton groups
136 multiplied by a factor of 1.7 mg-Chl/mmol-N (Thomas et al., 1992). The calanoid copepod *C.*
137 *finmarchicus* generally dominates the mesozooplankton biomass (Møller and Nielsen, 2020) and
138 the physiological processes were parameterized according to previous studies (Møller et al.,
139 2012, 2016). The model considers the processes of nutrient uptake, growth, grazing, egestion,
140 respiration, recycling, mortality, particle sinking and seasonal mesozooplankton migration in the
141 water column and overwintering in bottom waters. NPP was estimated as daily means of
142 phytoplankton growth after subtracting respiration and integrated over 30 m depth corresponding
143 to the productive layer. The timing of the seasonal *C. finmarchicus* migration was calibrated
144 against in situ measurements of their vertical distribution over time (Møller and Nielsen, 2019).
145 Light attenuation (k_d) is a function of background attenuation (water turbidity, k_{db}) and
146 concentrations of detritus and Chl *a* (Maar et al., 2011). Turbidity is strongly correlated with
147 salinity and the background attenuation was described as a function of salinity: $k_{db}=0.80\text{-salinity}$
148 $\times 0.0288$ for salinity < 25 according to measurements across a salinity gradient in another
149 Greenland fjord, the Young Sound (Murray et al., 2015) and set to a constant of 0.08 m^{-1} for
150 salinity >25 according to monitoring data in the Disko Bay $69^\circ 14' \text{ N}$, $53^\circ 23' \text{ W}$ (data.g-e-m.dk,
151 <https://doi.org/10.17897/WH30-HT61>).

152 Light optimum was changed for both phytoplankton groups during calibration to fit with the
153 timing of the spring bloom (Appendix A). Background mortality of microzooplankton was
154 increased to account for other grazing pressure than from *C. finmarchicus*.

155 **2.3 Freshwater and nutrient discharge**

156 We used the MAR and RACMO regional climate model (RCM) runoff field to compute
157 freshwater discharge. Ice runoff is defined as ice melt + condensation – evaporation + liquid
158 precipitation – refreezing. Land runoff is computed similarly, but there is no ice melt term
159 (although there is snow melt). Daily simulations of runoff were routed at stream scale to coastal
160 outlets, where it is then called ‘discharge’. Precipitation onto the ocean surface is not included in
161 the calculations (Mankoff et al., 2020a). Within Disko Bay, 235 streams discharge liquid water,
162 of which 97.5 % of the water comes from just 30 streams.

163 Fourteen points were selected within the model domain to represent the freshwater inflow. The
164 locations were manually selected to best represent the location of the largest rivers/inflows and
165 the spatial distribution of freshwater inflow in the model domain. The inflow from the 30 largest
166 rivers were manually aggregated into the 14 point sources by evaluating the geographical
167 location in relation to the coastal layout. This land run-off was inserted into the nearest model
168 cell in the surface layer. Although subglacial discharge enters at depth, it rises up the ice front
169 within a few 10s to 100s of meters of the ice front and within the grid cell at the ice boundary
170 (1800 -3200 m wide) will reach its neutral isopycnal here assumed to be the surface layer
171 (Mankoff et al., 2016). Thus, ice runoff was inserted in the surface layer. Solid ice discharge was
172 computed from ice velocity, ice thickness, and ice density at marine terminating glaciers
173 (Mankoff et al., 2020b). Within our modelling area in Disko Bay four glaciers discharge icebergs
174 into fjords, of which the majority comes from Sermeq Kujalleq (Jakobshavn Isbræ). Solid ice
175 was inserted where glaciers terminate directly into fjords (Fig. 1). At these four localities with
176 marine terminating glaciers, the freshwater contribution as solid ice was assumed to be equally
177 distributed in the top 100 m assuming that the majority of the solid ice are small pieces that melts
178 quickly as evidenced by the lack of brash ice generally seen in Disko Bay. Thus, we do not
179 consider the large icebergs calved by Sermeq Kujalleq and their input of freshwater along the
180 route in the bay. Land discharge of nitrate, phosphate, and silicate at the 14 point sources was

181 assumed to be constant in time with concentrations of 1.25, 0.20 and 10.88 mmol m⁻³,
182 respectively (Hopwood et al., 2020).

183 **2.4 Hydrodynamic open boundary and initial data**

184 At the semi-circular open boundary towards the Baffin Bay, the model was forced with ocean
185 velocities, water level, salinity, and temperature obtained from a coupled ocean- and sea ice
186 model (Madsen et al., 2016) provided by the Danish Meteorological Institute (DMI). The DMI
187 model system consists of the HYbrid Coordinate Ocean Model (HYCOM, e.g., Chassignet et al.,
188 2007) and the Community Ice Code (CICE, (Hunke, 2001; Hunke and Dukowicz, 1997) coupled
189 with the Earth System modeling Framework (ESMF) coupler (Collins et al., 2005). The
190 HYCOM-CICE set-up at DMI covers the Arctic Ocean and the Atlantic Ocean, north of about
191 20°S, with a horizontal resolution of about 10 km. Further details on the HYCOM-CICE model
192 system can be found in Appendix B.

193 The 2D (water level) and 3D parameters were interpolated to match the open boundary in the
194 FlexSem Model setup using linear interpolation. Correspondingly, initial fields of temperature,
195 salinity and water level were interpolated from the HYCOM-CICE model output.

196 **2.5 Observed sea ice cover**

197 The long term sea ice cover within Disko Bay was extracted from the sea ice concentration data
198 provided by the EUMETSAT Ocean and Sea Ice Satellite Application Facility (OSISAF,
199 www.osi-saf.org, Lavergne et al., 2019) on a daily basis (AICE). The Disko Bay area is here
200 defined as longitude and latitude range between 54.0°W and 51.5°W and 68.7°N to 69.5°N
201 respectively. As the OSISAF product is seasonally quite noisy for low sea ice concentrations, we
202 made a cutoff at 40 percent before we take the mean for the entire area. The exact cut-off value
203 does not matter much on the resulting time series, as the freeze-up and melt-down period is quite
204 fast for the area. Furthermore, we obtained sea ice observations from the Greenland Ecosystem
205 Monitoring (GEM) program (<http://data.g-e-m.dk>, <https://doi.org/10.17897/SVR0-1574>) in
206 which ice coverage is registered daily by visual inspection from the laboratory building at
207 Copenhagen University's Arctic station in Qeqertarsuaq.

208 **2.6 Surface forcing data**

209 At the surface, the model was forced by sea ice concentration, wind drag and heat fluxes. The ice
210 cover percentage modifies the wind drag, heat balance and light penetration in the model. Glacier
211 ice cover was assumed to be present throughout the year in the Jakobshavn Isbræ near Ilulissat
212 with the ice edge located at the mouth of the fjord whereas land- and ice runoff were located at
213 the sub-arms of the fjord (Figure 1). The surface heat budget model estimating the heat flux
214 (long- and short-wave radiation) was forced by wind, 2 meter atmospheric temperature, cloud
215 cover, specific humidity and ice cover. Photosynthetically active radiation (PAR) was estimated
216 from the short-wave radiation assuming 43% to be available for photosynthesis (Zhang et al.,
217 2010). The atmospheric forcing was provided by DMI from the HIRLAM (Yang et al., 2005)
218 and HARMONIE (Yang et al., 2017; 2018) meteorological models using the configuration with
219 the best resolution available for our simulation period. The resolution was 15 km until May
220 2005, then increased to about 5 km until March 2017, and since then to 2.5 km. Ice cover was
221 obtained from the HYCOM-CICE model output.

222 **2.7 Biogeochemical open boundary and initial data**

223 Initial data and open boundary conditions for ecological variables were obtained from the pan-
224 Arctic ‘A20’ model at NIVA Norway. This was based on a 20 km-resolution ROMS ocean-sea
225 ice model (Shchepetkin and McWilliams, 2005, Roed et al., 2014) coupled to the ERSEM
226 biogeochemical model (Butenschön et al., 2016), run in hindcast mode and bias-corrected
227 towards a compilation of in situ observations (Palmer et al., 2019). This model provided bias-
228 corrected output for (nitrate, phosphate, silicate, dissolved oxygen) plus raw hindcast output for
229 ammonium, detritus (small, medium and large fractions), 6 groups of phytoplankton and 3
230 zooplankton groups. The picophytoplankton, Synechococcus, nano-, micro-phytoplankton and
231 prymnesiophyte biomasses from ERSEM were summed to provide data for the autotrophic
232 flagellate group in ERSEM, while the diatom functional group was the same in both models.
233 The detritus pool in ERSEM was the sum of the three detritus size fractions in ERSEM. The
234 A20 data were provided as weekly means on a 20 km grid and linearly interpolated to the
235 FlexSem grid. ERSEM provided data through 2014, then 2014 was repeated for the following
236 years.

237 2.8 Validation

238 For model calibration and validation of the seasonality, we used reported research observations
239 of temperature, salinity, nutrients (nitrate, silicate, phosphate), Chl *a* concentrations and
240 mesozooplankton biomass collected during short-term field campaigns at the Disko Bay station
241 69° 14' N, 53° 23' W from 2004 to 2012 (e.g.(Møller and Nielsen, 2019)). Furthermore, we used
242 observations of the same variables from the same station provided by the Greenland Ecological
243 Monitoring (GEM) program running since 2016 in the Disko Bay (data.g-e-m.dk). However, the
244 data coverage is highly sporadic between years and months, and we therefore created a monthly
245 climatology (2004-2018) for the best-sampled depth layer 0-20 m (Møller et al, 2022). This
246 climatology was compared with monthly means extracted from the model at the same location
247 and depth range where 2004 was used for model calibration and means from 2005 to 2018 for
248 model validation. Mesozooplankton biomass in the model was assumed to mainly represent the
249 copepods *Calanus* spp. and for the conversion from N to carbon (C) biomass, we used 12 g-C
250 mol⁻¹ and C:N= 6.0 mol-C mol-N⁻¹ (Swailethorp et al., 2011).

251 Additionally, the model was validated spatially using remote sensing (RS) data of sea surface
252 temperature (SST) and Chl *a* concentrations for spring (April to June) and summer (July to
253 September) for 2010 and 2017. RS data was obtained from the Copernicus Marine Service (ref
254 <https://marine.copernicus.eu>). For SST we used the L4 product
255 'SEAICE_ARC_PHY_CLIMATE_L4_MY_011_016-TDS', which has spatial resolution of 0.05
256 degree and daily time resolution. For Chl *a* we used the data service
257 'OCEANCOLOUR_ARC_CHL_L4_REP_OBSERVATIONS_009_088-TDS' (L4 product
258 based on the OC5CCI algorithm), which has a spatial resolution of 0.01 degree and monthly time
259 resolution. Chl *a* concentrations were log-transformed because they span several orders of
260 magnitude. For both SST and Chl *a* comparisons, the RS data were interpolated to cell center
261 points of the horizontal FlexSem grid using a bi-linear scheme. Validation was only performed at
262 spatial points, where RS data has at least one quality-accepted data entry (i.e. sufficient visibility
263 without ice and cloud cover) for the respective validation periods.

264 The model skill was assessed by different metrics. The Pearson correlation between observations
265 and model results was estimated for the seasonal data and spatial data assuming a significance
266 threshold of $p < 0.05$. The other metrics were:

267 Mean Error (ME) is the mean of the differences between observations x and model results y :

$$268 \quad ME = \frac{1}{N} \sum_{i=1}^N (y_i - x_i)$$

269 where N is the total number of data points. The Root Mean Square Error (RMSE) is the square
270 root of the mean squared error between x and y :

$$271 \quad RMSE = \sqrt{\frac{1}{N} \sum_{i=1}^N (y_i - x)^2}$$

272 The average cost function (cf) is defined as (Radach and Moll 2006):

$$273 \quad cf = \frac{1}{N} \sum_{i=1}^N \frac{|(y_i - x_i)|}{SD(x)}$$

274 Depending on the cf number, it is possible to assess the performance of the model as “very good”
275 (<1), “good” (1-2), “reasonable” (2-3), and “poor” (>3).

276 Microzooplankton data was available from the literature for 1996/97 (Levinsen and Nielsen,
277 2002) and April-May 2011 (Menden-Deuer et al., 2018). Thus, it was not possible to create a
278 climatology, but the available data was used for visual comparison with model data. Data from
279 Levinsen and Nielsen (2002) was depth integrated (g-C m^{-2}), and converted to mg-C m^{-3} by
280 assuming that the total biomass was distributed uniformly over the upper 25 m (Levinsen et al.,
281 2000). Data from Menden-Deuer (2018) was from fluorescence maximum, and this was assumed
282 to represent the upper 20 m. The conversion from nitrogen to carbon biomass was obtained from
283 the Redfield ratio= $6.625 \text{ mol-C mol-N}^{-1}$ and the mol weight of 12 g-C mol^{-1} .

284 **2.9 The impact of sea ice cover and discharge on primary productivity**

285 An overall indication of the relationship between NPP and sea ice cover and freshwater
286 discharge was obtained by Pearson product moment correlation analysis between annual
287 estimates of these for the entire Bay, as defined by the box in figure 1. We further evaluated the
288 impact of sea ice cover and freshwater discharge on the NPP on a spatial scale. To do this we
289 perform correlation analysis between the annual NPP and the average sea ice cover March-April
290 in each model grid cell for 2004-2018. To evaluate the impact of the discharge we performed
291 similar correlations with average annual surface salinity instead of sea ice cover. The

292 assumption behind the choice is that the surface salinity scales with the impact of freshwater
293 discharge.

294 To demonstrate the effect of sea ice cover and distance to the glacial outlet on the temporal
295 development of nitrogen concentration, Chl *a*, and NPP, two stations and two years with
296 different features were selected. The first station was located in the open bay and the other
297 station close to the Ilulissat Isfjord (Bay and Glacier station, Fig. 1). The two years 2010 and
298 2017 were chosen according to differences in both irradiance and sea ice cover, one (2010) with
299 low sea ice cover and high irradiance and the other (2017) with high sea ice cover and low
300 irradiance.

301 To further evaluate the impact of sea ice cover and freshwater discharge we performed some
302 simple “extreme” model scenarios (Table 1). We tested the potential effect on primary
303 productivity in 2010 (low sea ice cover) and 2017 (high sea ice cover) in scenarios with no sea
304 ice, no freshwater discharge or 2 times the reference discharge, as well as the combinations, by
305 changing the model forcing accordingly.

306 We furthermore for 2010 tested the impact of inserting the ice runoff at the glacier grounding
307 line instead of the surface layer where glaciers terminate directly into fjords (Fig. 1).

308 3 Results

309 3.1 Freshwater discharge and sea ice cover

310 50 years ago, the average annual liquid runoff from the ice sheet to the study area was generally
311 $\sim 1000 \text{ m}^{-3} \text{ s}^{-1}$ ($913 \pm 2214 \text{ SD m}^{-3} \text{ s}^{-1}$, 1958-1969), whereas during the last 20 years is has varied
312 between 2000 and 4500 $\text{m}^{-3} \text{ s}^{-1}$ ($2591 \pm 724 \text{ SD m}^{-3} \text{ s}^{-1}$, 2000-2019) (Fig. 2). The precipitation
313 over land has also increased from about 200 ($197 \pm 40 \text{ SD m}^{-3} \text{ s}^{-1}$) to 400-500 $\text{m}^{-3} \text{ s}^{-1}$ ($469 \pm 77 \text{ SD}$
314 $\text{m}^{-3} \text{ s}^{-1}$). The calving of solid ice from the glaciers has only been estimated for the last 30 years,
315 but it also shows an increasing trend although since the maximum in 2013, the production of ice
316 has been lower (Fig. 2). Thus, for all three sources of freshwater the overall long-term trend is an
317 increase, but for the model period between 2004 and 2018 no trend was evident (Fig. 3e). The
318 freshwater discharge from solid ice was relatively constant across the year, whereas the liquid
319 contribution peaked during summer, from June to August, and drops to almost zero in the winter
320 (Fig. 3f).

321 The sea ice cover in Disko Bay has generally decreased during the last 35 years (Fig. 2).
322 However, the last 15 years have been characterized by large interannual variation with some
323 years with virtually no ice and others with sea ice cover as in the 1990s. During the model period
324 the ice generally did not form before late December, and the maximum ice cover was seen in
325 March (Fig. 3)

326 **3.2 Validation of the model**

327 The seasonal timing and general level of temperature, salinity, nutrients, Chl *a* and
328 mesozooplankton agreed well with the data climatology from the field sampling south of Disko
329 Island (Fig. 4, Table 2). All correlations between observational and model data were significant
330 ($R > 0.82$). The model performance assessed by the average cost function *cf* was “very good” for
331 all parameters. Modelled Chl *a* showed highest interannual variability in spring and the
332 chlorophyll bloom was somewhat too weak (~30% less), and the winter silicate too high, relative
333 to the climatological mean observations.

334 The spatial distribution patterns of Chl *a* and temperature at the surface were compared to
335 satellite estimates for the two years 2010 and 2017 used in the scenarios representing low and
336 high sea ice cover, respectively (Table 3, Fig. C1). The correlations were significant for all
337 relations ($p < 0.01$), and the *cf* number was “very good” or “good” for all (Table 3). Surface
338 temperature tended to be higher in spring and lower in summer in the model compared to the
339 satellite estimates. Chl *a* concentrations were generally higher in the model than in the satellite
340 data, especially in spring 2017 (Fig. C1).

341 **3.3 Seasonal and spatial patterns of NPP in Disko Bay**

342 Primary production starts as sea ice cover decreases and irradiance increases in February (Fig. 3).
343 Extensive sea cover may reduce light availability in the water column and thereby limit
344 production, and the interannual variation in NPP is highest in April because of the variation in
345 sea ice cover, causing light availability in the water to vary accordingly. Highest NPP was in
346 May and June with about $800 \text{ mg-C m}^{-3} \text{ d}^{-1}$ when light influx was highest and sea ice was
347 entirely melted (Fig. 3).

348 The impact of sea ice is illustrated by comparing a year with low (2010) and high (2017) sea ice
349 cover, where the spring bloom is about 25-30 days earlier in 2010 than in 2017 (Fig. 5).

350 Comparing a station close to and far from the glacier illustrates the potential impact of the
351 freshwater peak in late summer, as NPP is 2-3 times higher during this period at the station close
352 to the glacier (Fig. 5).

353 Concerning the spatial distribution in the spring period (March to June), high NPP was seen
354 across the bay, with the lowest values found southeast of the Disko Island and southwest of the
355 Bay following the bathymetry. In the later summer period (July to October), primary production
356 was more confined to the coast (Fig. 6).

357 **3.4 Annual variability of NPP**

358 The annual average NPP in the Bay estimated from the model varied between 90 and 147 g-C
359 m⁻² year⁻¹ with an average of 129±16 (SD) (Fig. 3). Generally, years with high sea ice cover in
360 spring had lower average annual NPP (Fig. 3, Pearson product moment correlation coefficient r
361 = -0.63, $p=0.01$), while higher discharge was associated with higher annual primary productivity
362 (Fig. 3, $r = 0.51$, $p=0.05$).

363 To evaluate the spatial dependency, we performed an analysis of the correlation between the sea
364 ice cover in March to April and the annual NPP in each model grid cell. This showed a negative
365 relationship widespread in the model domain, i.e. the more sea ice, the lower NPP (Fig. 7). One
366 exception was in the south part of the model domain, where the correlation was positive. The
367 impact of the freshwater discharge on the NPP was generally positive in areas up to ~50 km from
368 the discharge and additionally in the northern part of Disko Bay, as reflected by the negative
369 correlation to surface salinity in these areas (Fig. 7).

370 **3.5 Model scenarios with sea ice cover and discharge**

371 We studied some simple model scenarios where sea ice cover was assumed to be zero and the
372 discharge was either doubled or cut off, with basis in 2010 and 2017, which had low and high sea
373 ice cover, respectively, and opposite discharge (Fig. 3). These scenarios underline the
374 complexity of the dynamics of the system, with some areas experiencing increased NPP while
375 others experience a decrease (Figs. 8, 9). Furthermore, it allows us to evaluate the impact of the
376 uncertainty of actual freshwater runoff. The year 2017 had relatively high and late ice cover (Fig.
377 3) and applying a scenario of no ice leads to an increase in bay-scale annual NPP of 34 %,
378 although spatial variability is high and annual NPP changes vary between -20% and 98% (Fig.

379 9). For 2010, a year that already had low sea ice cover, the same scenario led to minor changes in
380 the annual NPP on bay scale (2 %, Fig. 8). For both years, the omission of freshwater discharge
381 generally led to a decrease in annual NPP; this effect was small on the bay scale (-2 to 0%), but
382 reached -64% in near-coastal areas under glacial/runoff influence. Similarly, the effect of
383 doubling of the discharge was minor on the bay scale (0-1%), but reached up to 55 and 68 %
384 NPP increase in runoff-influenced areas in 2010 and 2017, respectively. The effects of sea ice
385 and freshwater discharge changes combined in an approximately additive manner (Figs. 8, 9).
386 When the forcing from sea ice cover and freshwater discharge were set to be zero in 2010 and
387 2017, NPP in 2017 was were still 20% smaller than the 2010. This illustrates the importance of
388 other factors for NPP like wind, cloud cover and inflow to the bay.

389 Horizontal (East-West) current velocity profiles at the ice edge (water depth of 241 m) of
390 Jakobshavn Isbræ showed an outgoing westly direction with highest outflow at 150-200 m depth
391 from March to October (Figure C4a). Vertical velocities showed an upward transport with
392 highest values close to the bottom at 190-216 m depth (Figure C4b). The scenario with no runoff
393 (noQNP) showed weaker horizontal transports and less upwelling at the ice edge (Figure C4).
394 When ice run-off was released at the glacier grounding line instead at the surface, only a small
395 increase of horizontal and vertical velocities was found at 90-200 m depth relative to the
396 baseline. In addition, a small spatial displacement of the primary production was seen (Fig C5).
397 The stratification and vertical distribution of nutrients, Chl *a* and primary production were not
398 changing much, just establishing a bit further offshore in the late summer months (Fig C3+C6).
399 The effect on the bay primary productivity is only minor (<1%).

400 4 Discussion

401 Primary productivity is an essential ecosystem service that shapes the structure of the marine
402 ecosystem and fuels higher trophic levels such as fish that is vital for the Greenlandic society. It
403 is therefore important to estimate potential outcomes for primary production under the continued
404 warming and subsequent ice melt. For the coastal ocean, especially around Greenland, it is
405 imperative to quantify how changes in sea ice cover and run-off combine to determine the
406 availability of the two key resources, light and nitrate, determining the magnitude and phenology
407 of primary production. Sea ice cover and run-off influence light and nitrate availability through
408 several intermediate processes, and their peak impact often occurs in different areas and in

409 different months. The spatial-temporal variability and complexity of processes involved requires
410 an approach where detailed *in situ* observations are combined with remote sensing and
411 modelling. The present study is to our knowledge the first attempt to apply this approach for
412 coastal Greenland.

413 Our model results show that reduction in spring sea ice cover changes the plankton phenology
414 but also increases the magnitude of annual production in Disko Bay. This suggests that there is a
415 replenishment of nitrate into the photic zone to sustain the continued productivity beyond the
416 initial depletion following the spring bloom. Part of the nitrate input is coupled to the run-off, but
417 the high modelled productivity from April to July, when liquid run-off is limited suggest that
418 vertical mixing fueled by wind and tide is important. That less sea ice cover will lead to
419 increased NPP is in agreement with other studies from the open Arctic areas (Arrigo and van
420 Dijken, 2015; Vernet et al., 2021). In other Greenland fjords, the turbulence driving vertical
421 mixing has been shown to be very low (Bendtsen et al., 2021; Randelhoff et al., 2020), but is
422 seems likely that the open Disko Bay with a tidal amplitude of up to 3 m (Thyrring et al., 2021)
423 could have an efficient vertical flux of nitrate into the photic zone.

424 Our study site was chosen because the Disko Bay in mid-west Greenland is considered a hot-spot
425 for marine biodiversity and fisheries, and because it is an area where both sea ice cover and
426 glacial run-off are likely to be important for productivity. But regional variability is high across
427 the coastal ocean around Greenland. For example, ice cover is very limited in most of SW
428 Greenland and is unlikely to drive changes in future primary production, whereas glacial run-off
429 is less in NE Greenland compared to the rest of Greenland. Furthermore, the dominance of land
430 or marine terminating glaciers as in Disko Bay will be important for the outcome of increased
431 glacial run-off on individual fjord scale (Hopwood et al., 2020; Lydersen et al., 2014). Finally,
432 winter concentration of nitrate and vertical gradients in summer differ between the East and West
433 coast, with low nitrate content in the East Greenland Current generally causing lower
434 productivity compared to West Greenland (Vernet et al. 2021).

435 **4.1 Phenology of primary producers**

436 A main advantage of the model is that it allows us to estimate the productivity with a higher
437 temporal and spatial resolution than would be possible from measurements alone. The sea ice
438 cover had a clear effect on the spring NPP. When sea ice cover is low, spring NPP is starting

439 earlier compared to years with high sea ice cover, and the largest variation in NPP between years
440 is seen in the spring months (Fig. 3). The performed scenarios support the importance of sea ice
441 cover, i.e. the absence of sea ice leads to a considerable increase in the annual NPP on bay scale
442 (Fig. 9). Potentially, NPP could start as early as February if considering the light availability.
443 However, for NPP to increase would also require the water column to stabilize, i.e. wind mixing
444 would need to be sufficiently low (Tremblay et al., 2015). In contrast, the timing of the formation
445 of the sea ice in fall is not important for the primary productivity, since the sea ice in Disko Bay
446 does not form before the light has largely disappeared. This is in contrast to high Arctic systems
447 where sea ice normally forms earlier and a delay in the formation of sea ice in fall may result in
448 autumn blooms (Ardyna et al., 2014).

449 **4.2 Spatial distribution of NPP**

450 In our analysis, we see a positive effect of the freshwater discharge on the primary productivity
451 locally and during the summer months. This effect is related to the upwelling that is enhanced by
452 the freshwater discharge (Fig. C2, C3). The nutrient concentration in the discharge (1.25 μM ,
453 Hopwood et al., 2020) is lower than the average concentration in the upper 30 m during summer
454 at the station near the glacier (e.g. $\sim 4 \mu\text{M NO}_3$) (Fig. 7), and will therefore not lead to increased
455 NPP. This is in accordance with the general picture from glacial affected environments. River
456 discharge may on the other hand carry higher nutrient concentrations, particularly of nitrogen
457 (Hopwood et al., 2019).

458 We used two approaches to evaluate the spatial scale of the effect freshwater discharge. The
459 correlation analyses using salinity as a proxy for the discharge (Fig. 7) suggest that the discharge
460 may influence ~ 50 km away from the source. The scenarios where we alter the discharge
461 suggest that the effect is only a couple of percent considering NPP on the Bay scale, whereas on
462 a more local scale near the glacier the importance is higher (-64% to 147%, Fig. 8 and 9).

463 Godthåbsfjord is situated further south at the west coast of Greenland and is fjord system less
464 directly affected by the ocean dynamics than the open Disko Bay. Here glacial runoff has been
465 suggested to affect the seasonal development of phytoplankton 120 km away from the glacier
466 (Juul-Pedersen et al., 2015). Furthermore, it was found that 1-11% of the NPP in the Fjord
467 systems is supported by entrainment of N by the three marine terminating glaciers (Meire et al.,
468 2017). Considering only the parts of the fjord directly impacted by the discharge the estimate

469 were 3 times higher (Hopwood et al., 2020). Analyses from Svalbard fjords impacted by glacial
470 discharge showed positive spatiotemporal associations of Chl *a* with glacier runoff for 7 out of
471 14 primary hydrological regions but only within 10 km distance from the shore (Dunse et al.,
472 2022).

473 The modelling in this study allows us to evaluate the combined effect of changes in sea cover
474 and freshwater discharge in the coastal ecosystem of the Disko Bay. Importantly, this study also
475 illustrates that within the Arctic coastal zone, the combination of different climate change effects
476 may lead to different responses within relatively small distances. Thus, while we can suggest a
477 general increasing trend in the NPP, this may not be evident when considering local
478 observations. This is important to consider when planning and evaluating field investigations.

479 **4.3 Modelled NPP versus other estimates**

480 The biogeochemical model was validated using all available observations. These are all
481 concentrations (nutrients) or standing stocks (phytoplankton, zooplankton). The satisfactory
482 validation is an indication that the rates are also adequately described. Still, it is desirable also to
483 have direct comparison with rate measurements. There are no available NPP measurements for
484 our modelling period. However, data are available from 1973-1975 (Andersen, 1981) and
485 1996/97 (Levinsen and Nielsen, 2002) and 2003 (Sejr et al., 2007). The data from 1996/97 were
486 *in situ* bottle incubations in the upper 30 m, and no further information on methodology was
487 given (referred to as unpublished). The sea ice cover was generally high in Disko Bay at that
488 time (Fig. 4) and we therefore compare the seasonal development to our model estimates from
489 2017, a year with extensive sea ice cover. The estimate of the annual production from 1996/97
490 was 28 gC m⁻² d⁻¹ less than half the estimate from 1970s of 70 gC m⁻² d⁻¹, and the modeling
491 estimates from 2017 of 82 gC m⁻² d⁻¹ at the same station. The measurements do, however, both
492 agree with the model on the seasonal timing of NPP with an increase in NPP between March and
493 April, and the Pearson correlation coefficients between measurements and model results were
494 0.84, p<0.001 (1996/7) and 0.69, p<0.05 (1973-75). Data from 2003 (Sejr et al., 2007) are from a
495 shallow cove only in two shorter periods, but the production of 195 mgC m⁻² d⁻¹ in April aligns
496 well with our estimates, whereas the value in September 27 mgC m⁻² d⁻¹ is somewhat lower.

497 Average estimates of NPP from Arctic glacial fjords with marine terminating glaciers are
498 reported to be 400-800 mg-C m⁻² d⁻¹ during July to September (Hopwood et al., 2020). In the
499 Arctic Ocean, shelf regions estimates from satellite observations are 400-1400 mgC m⁻² d⁻¹ in
500 April to September during 1998 to 2006 (Pabi et al., 2008). Thus, overall, our model estimates of
501 NPP in Disko Bay of 378-815 mgC m⁻² d⁻¹ between April and September (Fig. 3) are in the same
502 range as other estimates.

503 In another modelling study, a physically-biologically coupled, regional 3D ocean model
504 (SINMOD) was compared with ocean color remote sensing (OCRS). Both OCRS and SINMOD
505 provided similar estimates of the timing and rates of productivity in of the shelves around
506 Greenland (Vernet et al., 2021). In the region including Disko Bay, the modelled NPP was
507 generally suggested to be much lower (20-23 gC m⁻² yr⁻¹) than our estimate (90-147 gC m⁻² yr⁻¹)
508 and the bloom was suggested to generally start later (late May). However, their model mainly
509 covered the shelf area north of Disko Bay and did not resolve the plume outside the ice fjord.
510 Moreover, the estimates from OCRS (50 gC m⁻² yr⁻¹) were about double the modelled values,
511 and furthermore could only be recorded after ice break-up when the bloom was already on its
512 maximum (Vernet et al., 2021), suggesting that it could be much higher.

513 **4.4 Uncertainty and potential model improvement**

514 We model the impact of turbidity on light conditions in the water column as a simple relationship
515 between salinity and light attenuation. More sophisticated light models may be applied in future
516 models (Murray et al., 2015). However, in a relatively open water system like Disko Bay, the
517 effect of increased light attenuation due to increased turbidity is only expected within 5-10
518 kilometers of the glacial outlet. Moreover, we do not expect an impact on the total NPP in the
519 bay since the nutrients will anyway be used within the bay. A comparison between the spatial
520 distribution of surface Chl *a* assessed by satellite and the model showed a significant correlation
521 and the model performance were evaluated good to excellent (Table 3). Still, visual inspections
522 of the two maps suggest that the effect of the discharge on the Chl *a* spatial distribution were
523 more local and concentrated in the model than what is suggested by the satellite estimates (Fig.
524 C1). Thus, a higher precision in the spatial distribution of the phytoplankton may be achieved by
525 improving the model parametrization of light attenuation, e.g. by inserting a passive tracer
526 reflecting the turbidity in melt water. A more dynamic description of acclimation of primary

527 productivity to different light under nutrient conditions (Ross and Geider, 2009), may be
528 achieved by implementing variable element ratios (e.g., C:N) of phytoplankton instead of the
529 fixed ratios in the current model. The uncertainty in the different freshwater discharge source
530 may impact our estimates of marine productivity differently. Liquid runoff uncertainty and errors
531 are more likely to be random than bias, and when averaged together (over large spatial areas or
532 times) the uncertainty is reduced (Mankoff et al., 2020b). Conversely, solid ice discharge
533 uncertainty comes primarily from unknown ice thickness, which is time-invariant and therefore
534 must be treated as a bias term (Mankoff et al., 2020a). It does not reduce when averaged in space
535 or time.

536 We do not specifically model the subglacial discharge of freshwater from the marine terminating
537 glaciers or from melting of the numerous large icebergs in the bay. Instead, the freshwater
538 discharge from solid ice was distributed equally across the upper 100 m in the locations where
539 marine terminating glaciers were present. Subglacial discharge that enters at depth, will rise up
540 the ice front within a few 10s to 100s of meters of the ice front (Mankoff et al., 2016), which is
541 within the grid cell size of the model. We therefor inserted ice discharge in the model surface
542 layer that was found to be fully mixed in the water column during transport towards the ice edge.
543 At the ice edge of the Jakobshavn Isbræ, modelled velocity profiles confirmed a bottom
544 upwelling due to higher outgoing water transport at the bottom of the glacier (Figure C4a, b) in
545 accordance with previous studies of marine terminating glaciers (Hopwood et al. 2020). In the
546 scenario with no runoff (noQNP), the outgoing transport and vertical velocities at depths below
547 100m was severely reduced confirming the importance of ice discharge for the observed
548 dynamic (Hopwood et al. 2020). When the discharge instead was inserted at the grounding line
549 of the marine terminating glaciers, there was a limited increase in the vertical velocity marginal
550 (Figure C5b). Similarly, there was only a slight displacement of the phytoplankton bloom to
551 further offshore and very limited changes in the stratification and vertical distribution of
552 nutrients, Chl *a* and NPP (Fig C5+C6). The effect of the primary productivity of the Bay was
553 <1%.

554 To be able to resolve the small-scale mixing between sub-glacial discharge and ambient fjord
555 water in the plume directly in front of the glacier a higher model resolution will be needed. A
556 study from another Greenland fjord suggests efficient mixing near the glacial terminus, which

557 means that the freshwater fraction in the surface water near the glacial front is only 5-7%, which
558 indicates that the mixing ratio between sub-glacial discharge and fjord water is 1 liter of
559 meltwater to 13-16 liters of fjord water (Mortensen et al., 2020). The capacity of buoyancy
560 driven upwelling of subglacial discharge to supply nutrients to the photic zone depends on
561 several factors including the depth of the freshwater input and the density and nutrient content of
562 the ambient fjord water. Our approach to distribute the solid ice freshwater input in the upper
563 100 m and the ice runoff in the surface layer is a first attempt to simulate the average conditions
564 across the study area. We were able to reproduce the general pattern of upwelling (Fig C2+C3)
565 and spatial dynamics of productivity, but the magnitude could be under- or overestimated.
566 Models of high spatial and process resolution are mainly developed to describe the transports of
567 heat and salt to glacial ice, in order to estimate the melt (Burchard et al., 2022). If the focus is to
568 describe the fine scale processes in front of the glacier, the development within these models
569 may in the future be implemented in ocean models.

570 **4.5 Conclusions**

571 Two important drivers of changes in the Arctic coastal ecosystems are sea ice cover and glacial
572 freshwater discharge. This modelling study estimates the response of the pelagic net primary
573 (NPP) production to changes in sea ice cover and freshwater run-off in Disko Bay, West
574 Greenland, from 2004 to 2018. The difference in annual production between the year with lowest
575 and highest annual NPP was 63%. Our analysis suggests that sea ice cover was the more
576 important of the two drivers of annual NPP through its effect on spring timing and annual
577 production. Freshwater discharge, on the other hand, had a strong impact on the summer NPP
578 near to the glacial outlet. Hence decreasing ice cover and more discharge can work
579 synergistically and increase productivity of the coastal ocean around Greenland.

580 **5 Code/Data availability**

581 The FlexSem source code and precompiled source code for Windows (GNU General Public
582 License) can be downloaded at <https://marweb.bios.au.dk/Flexsem>. The specific code for the
583 Disko set-up can be downloaded on Zenodo.org (Larsen, 2022; Maar et al., 2022).

584 6 Author contribution

585 EFM, MAM, MS conceptualized the study. MAM, JL, EFM was responsible for the FLEXSEM
586 development and validation, MHR for HYCOM-CICE, PW for the Arctic ‘A20’ model, KM for
587 MAR/ RACMO, and AC for the remote sensing data. MAM and EFM analyzed, synthesized and
588 visualized the data. EFM prepared the initial draft, and all authors contributed to review and
589 editing.

590 7 Competing interests

591 The authors declare that they have no conflict of interest.

592 8 Acknowledgements

593 This research has been supported by the Programme for Monitoring of the Greenland Ice Sheet
594 (PROMICE) and the European Union's Horizon 2020 research and innovation program
595 (INTAROS, grant no. 727890), and the Danish Environmental Protection Agency (MST-113
596 00095 and j-nr 2019 - 8443). MHR was funded by the Danish State through the National Centre
597 for Climate Research. PW was funded by the Joint Programming Initiative Healthy and
598 Productive Seas and Oceans (JPI Oceans) project CE2COAST and the EU Horizons 2020 project
599 FutureMARES, and used resources provided by the Norwegian Metacenter for Computational
600 Science and Storage Infrastructure (Notur/Norstore projects nn9490k, nn9630k, and ns9630k).
601 Data from the Greenland Ecosystem Monitoring Programme were provided by the Department
602 of Ecoscience, Aarhus University, Denmark, in collaboration with the Department of
603 Geosciences and Natural Resource Management, Copenhagen University, Denmark. The authors
604 are solely responsible for all results and conclusions presented, and they do not necessary reflect
605 the position of the Danish Ministry of the Environment or the Greenland Government.

606 **References**

- 607 Andersen, O. G. N.: The annual cycle of phytoplankton primary production and hydrography in
608 the Disko Bugt area, West Greenland., *Meddelelser om Gronland, Biosci.*, 6, 1981.
- 609 von Appen, W. J., Waite, A. M., Bergmann, M., Bienhold, C., Boebel, O., Bracher, A., Cisewski,
610 B., Hagemann, J., Hoppema, M., Iversen, M. H., Konrad, C., Krumpen, T., Lochthofen, N.,
611 Metfies, K., Niehoff, B., Nöthig, E. M., Purser, A., Salter, I., Schaber, M., Scholz, D., Soltwedel,
612 T., Torres-Valdes, S., Wekerle, C., Wenzhöfer, F., Wietz, M. and Boetius, A.: Sea-ice derived
613 meltwater stratification slows the biological carbon pump: results from continuous observations,
614 *Nat. Commun.*, 12(1), 1–16, doi:10.1038/s41467-021-26943-z, 2021.
- 615 Ardyna, M., Babin, M., Gosselin, M., Devred, E., Rainville, L. and Tremblay, J.-É.: Recent
616 Arctic Ocean sea ice loss triggers novel fall phytoplankton blooms, *Geophys. Res. Lett.*, 41(17),
617 6207–6212, doi:10.1002/2014GL061047, 2014.
- 618 Ardyna, M., Mundy, C. J., Mayot, N., Matthes, L. C., Oziel, L., Horvat, C., Leu, E., Assmy, P.,
619 Hill, V., Matrai, P. A., Gale, M., Melnikov, I. A. and Arrigo, K. R.: Under-Ice Phytoplankton
620 Blooms: Shedding Light on the “Invisible” Part of Arctic Primary Production, *Front. Mar. Sci.*,
621 7(November), 1–25, doi:10.3389/fmars.2020.608032, 2020.
- 622 Arrigo, K. R. and van Dijken, G. L.: Continued increases in Arctic Ocean primary production,
623 *Prog. Oceanogr.*, 136, 60–70, doi:10.1016/j.pocean.2015.05.002, 2015.
- 624 Bendtsen, J., Rysgaard, S., Carlson, D. F., Meire, L. and Sejr, M. K.: Vertical Mixing in
625 Stratified Fjords Near Tidewater Outlet Glaciers Along Northwest Greenland, *J. Geophys. Res.*
626 *Ocean.*, 126(8), 1–15, doi:10.1029/2020JC016898, 2021.
- 627 Bitz, C. M. and Lipscomb, W. H.: An energy-conserving thermodynamic model of sea ice, *J.*
628 *Geophys. Res. Ocean.*, 104(C7), 15669–15677, doi:10.1029/1999jc900100, 1999.
- 629 Butenschön, M., Clark, J., Aldridge, J. N., Icarus Allen, J., Artioli, Y., Blackford, J., Bruggeman,
630 J., Cazenave, P., Ciavatta, S., Kay, S., Lessin, G., Van Leeuwen, S., Van Der Molen, J., De
631 Mora, L., Polimene, L., Saille, S., Stephens, N. and Torres, R.: ERSEM 15.06: A generic model
632 for marine biogeochemistry and the ecosystem dynamics of the lower trophic levels, *Geosci.*
633 *Model Dev.*, 9(4), 1293–1339, doi:10.5194/gmd-9-1293-2016, 2016.

634 Chassignet, E. P., Hurlburt, H. E., Smedstad, O. M., Halliwell, G. R., Hogan, P. J., Wallcraft, A.
635 J., Baraille, R. and Bleck, R.: The HYCOM (HYbrid Coordinate Ocean Model) data assimilative
636 system, *J. Mar. Syst.*, 65(1-4 SPEC. ISS.), 60–83, doi:10.1016/j.jmarsys.2005.09.016, 2007.

637 Cohen, J., Zhang, X., Francis, J., Jung, T., Kwok, R., Overland, J., Ballinger, T. J., Bhatt, U. S.,
638 Chen, H. W., Coumou, D., Feldstein, S., Gu, H., Handorf, D., Henderson, G., Ionita, M.,
639 Kretschmer, M., Laliberte, F., Lee, S., Linderholm, H. W., Maslowski, W., Peings, Y., Pfeiffer,
640 K., Rigor, I., Semmler, T., Stroeve, J., Taylor, P. C., Vavrus, S., Vihma, T., Wang, S., Wendisch,
641 M., Wu, Y. and Yoon, J.: Divergent consensuses on Arctic amplification influence on
642 midlatitude severe winter weather, *Nat. Clim. Chang.*, 10(1), 20–29, doi:10.1038/s41558-019-
643 0662-y, 2020.

644 Collins, N., Theurich, G., DeLuca, C., Suarez, M., Trayanov, A., Balaji, V., Li, P., Yang, W.,
645 Hill, C. and da Silva, A.: Design and implementation of components in the Earth System
646 Modeling Framework, *Int. J. High Perform. Comput. Appl.*, 19(3), 341–350,
647 doi:10.1177/109434200505056120, 2005.

648 Dai, A. and Trenberth, K. E.: Estimates of freshwater discharge from continents: Latitudinal and
649 seasonal variations, *J. Hydrometeorol.*, 3(6), 660–687, doi:10.1175/1525-
650 7541(2002)003<0660:EOFDfC>2.0.CO;2, 2002.

651 Dee, D. P., Uppala, S. M., Simmons, A. J., Berrisford, P., Poli, P., Kobayashi, S., Andrae, U.,
652 Balmaseda, M. A., Balsamo, G., Bauer, P., Bechtold, P., Beljaars, A. C. M., van de Berg, L.,
653 Bidlot, J., Bormann, N., Delsol, C., Dragani, R., Fuentes, M., Geer, A. J., Haimberger, L., Healy,
654 S. B., Hersbach, H., Hólm, E. V., Isaksen, L., Kållberg, P., Köhler, M., Matricardi, M., McNally,
655 A. P., Monge-Sanz, B. M., Morcrette, J. J., Park, B. K., Peubey, C., de Rosnay, P., Tavolato, C.,
656 Thépaut, J. N. and Vitart, F.: The ERA-Interim reanalysis: Configuration and performance of the
657 data assimilation system, *Q. J. R. Meteorol. Soc.*, 137(656), 553–597, doi:10.1002/qj.828, 2011.

658 Dunse, T., Dong, K., Aas, K. S. and Stige, L. C.: Regional-scale phytoplankton dynamics and
659 their association with glacier meltwater runoff in Svalbard, *Biogeosciences*, 19(2), 271–294,
660 doi:10.5194/bg-19-271-2022, 2022.

661 Egbert, G. D. and Erofeeva, S. Y.: Efficient inverse modeling of barotropic ocean tides, *J.*
662 *Atmos. Ocean. Technol.*, 19(2), 183–204, doi:10.1175/1520-

663 0426(2002)019<0183:EIMOBO>2.0.CO;2, 2002.

664 Gladish, C. V., Holland, D. M. and Lee, C. M.: Oceanic Boundary Conditions for Jakobshavn
665 Glacier. Part II: Provenance and Sources of Variability of Disko Bay and Ilulissat Icefjord
666 Waters, 1990-- 2011, *J. Phys. Oceanogr.*, 45(2003), 33–63, doi:10.1175/JPO-D-14-0045.1, 2015.

667 Hansen, B. U., Elberling, B., Humlum, O. and Nielsen, N.: Meteorological trends (1991–2004) at
668 Arctic Station, Central West Greenland (69°15'N) in a 130 years perspective, *Geogr. Tidsskr. J.*
669 *Geogr.*, 106(1), 45–55, doi:10.1080/00167223.2006.10649544, 2006.

670 Hernes, P. J., Tank, S. E., Sejr, M. K. and Glud, R. N.: Element cycling and aquatic function in a
671 changing Arctic, *Limnol. Oceanogr.*, 66(S1), S1–S16, doi:10.1002/lno.11717, 2021.

672 Hibler, W. D.: A Dynamic Thermodynamic Sea Ice Model, *J. Phys. Oceanogr.*, 9(4),
673 doi:10.1175/1520-0485(1979)009<0815:adtsim>2.0.co;2, 1979.

674 Holding, J. M., Markager, S., Juul-Pedersen, T., Paulsen, M. L., Møller, E. F., Meire, L. and
675 Sejr, M. K.: Seasonal and spatial patterns of primary production in a high-latitude fjord affected
676 by Greenland Ice Sheet run-off, *Biogeosciences*, 16(19), doi:10.5194/bg-16-3777-2019, 2019.

677 Hopwood, M. J., Carroll, D., Browning, T. J., Meire, L., Mortensen, J., Krisch, S. and
678 Achterberg, E. P.: Non-linear response of summertime marine productivity to increased
679 meltwater discharge around Greenland, *Nat. Commun.*, 9(1), doi:10.1038/s41467-018-05488-8,
680 2018.

681 Hopwood, M. J., Carroll, D., Dunse, T., Hodson, A., Holding, J. M., Iriarte, J. L., Ribeiro, S.,
682 Achterberg, E. P., Cantoni, C., Carlson, D. F., Chierici, M., Clarke, J. S., Cozzi, S., Fransson, A.,
683 Juul-Pedersen, T., Winding, M. S. and Meire, L.: Review Article: How does glacier discharge
684 affect marine biogeochemistry and primary production in the Arctic?, *Cryosph. Discuss.*, (June),
685 1–51, doi:10.5194/tc-2019-136, 2019.

686 Hopwood, M. J., Carroll, D., Dunse, T., Hodson, A., Holding, J. M., Iriarte, J. L., Ribeiro, S.,
687 Achterberg, E. P., Cantoni, C., Carlson, D. F., Chierici, M., Clarke, J. S., Cozzi, S., Fransson, A.,
688 Juul-Pedersen, T., Winding, M. H. S. and Meire, L.: Review article: How does glacier discharge
689 affect marine biogeochemistry and primary production in the Arctic?, *Cryosphere*, 14(4), 1347–
690 1383, doi:10.5194/tc-14-1347-2020, 2020.

691 Høyer, J. L., Karagali, I., Dybkjær, G. and Tonboe, R.: Multi sensor validation and error
692 characteristics of Arctic satellite sea surface temperature observations, *Remote Sens. Environ.*,
693 121, 335–346, doi:10.1016/j.rse.2012.01.013, 2012.

694 Høyer, J. L., Le Borgne, P. and Eastwood, S.: A bias correction method for Arctic satellite sea
695 surface temperature observations, *Remote Sens. Environ.*, 146, 201–213,
696 doi:10.1016/j.rse.2013.04.020, 2014.

697 Hunke, E. C.: Viscous-Plastic Sea Ice Dynamics with the EVP Model: Linearization Issues, *J.*
698 *Comput. Phys.*, 170(1), 18–38, doi:10.1006/jcph.2001.6710, 2001.

699 Hunke, E. C. and Dukowicz, J. K.: An elastic-viscous-plastic model for sea ice dynamics, *J.*
700 *Phys. Oceanogr.*, 27(9), 1849–1867, doi:10.1175/1520-
701 0485(1997)027<1849:AEVPMF>2.0.CO;2, 1997.

702 Ji, R., Jin, M. and Varpe, Ø.: Sea ice phenology and timing of primary production pulses in the
703 Arctic Ocean., *Glob. Chang. Biol.*, 19(3), 734–41, doi:10.1111/gcb.12074, 2013.

704 Juul-Pedersen, T., Arendt, K. E., Mortensen, J., Blicher, M. E., S??gaard, D. H. and Rysgaard,
705 S.: Seasonal and interannual phytoplankton production in a sub-Arctic tidewater outlet glacier
706 fjord, SW Greenland, *Mar. Ecol. Prog. Ser.*, 524(MARCH), 27–38, doi:10.3354/meps11174,
707 2015.

708 Kjeldsen, K. K., Korsgaard, N. J., Bjørk, A. A., Khan, S. A., Box, J. E., Funder, S., Larsen, N.
709 K., Bamber, J. L., Colgan, W., Van Den Broeke, M., Siggaard-Andersen, M. L., Nuth, C.,
710 Schomacker, A., Andresen, C. S., Willerslev, E. and Kjær, K. H.: Spatial and temporal
711 distribution of mass loss from the Greenland Ice Sheet since AD 1900, *Nature*, 528(7582), 396–
712 400, doi:10.1038/nature16183, 2015.

713 Large, W. G. and Yeager, S. G.: The global climatology of an interannually varying air - Sea
714 flux data set, *Clim. Dyn.*, 33(2–3), 341–364, doi:10.1007/s00382-008-0441-3, 2009.

715 Larsen, J. (2022). FlexSem source code (2022-01-31). Zenodo.
716 <https://doi.org/10.5281/zenodo.7124459>

717 Lavergne, T., Macdonald Sørensen, A., Kern, S., Tonboe, R., Notz, D., Aaboe, S., Bell, L.,
718 Dybkjær, G., Eastwood, S., Gabarro, C., Heygster, G., Anne Killie, M., Brandt Kreiner, M.,

719 Lavelle, J., Saldo, R., Sandven, S. and Pedersen, L. T.: Version 2 of the EUMETSAT OSI SAF
720 and ESA CCI sea-ice concentration climate data records, *Cryosphere*, 13(1), doi:10.5194/tc-13-
721 49-2019, 2019.

722 Leu, E., Mundy, C. J. J., Assmy, P., Campbell, K., Gabrielsen, T. M. M., Gosselin, M., Juul-
723 Pedersen, T. and Gradinger, R.: Arctic spring awakening - Steering principles behind the
724 phenology of vernal ice algal blooms, *Prog. Oceanogr.*, 139, 151–170,
725 doi:10.1016/j.pocean.2015.07.012, 2015.

726 Levinsen, H. and Nielsen, T. G.: The trophic role of marine pelagic ciliates and heterotrophic
727 dinoflagellates in arctic and temperate coastal ecosystems: A cross-latitude comparison, *Limnol.*
728 *Oceanogr.*, 47(2), 427–439, doi:10.4319/lo.2002.47.2.0427, 2002.

729 Levinsen, H., Nielsen, T. G. and Hansen, B. W.: Annual succession of marine pelagic protozoans
730 in Disko Bay, West Greenland, with emphasis on winter dynamics, *Mar. Ecol. Prog. Ser.*, 206,
731 119–134, doi:10.3354/meps206119, 2000.

732 Lovejoy, C., Vincent, W. F., Bonilla, S., Roy, S., Martineau, M. J., Terrado, R., Potvin, M.,
733 Massana, R. and Pedrós-Alió, C.: Distribution, phylogeny, and growth of cold-adapted
734 picoplankton in arctic seas, *J. Phycol.*, 43(1), 78–89, doi:10.1111/j.1529-
735 8817.2006.00310.x, 2007.

736 Lydersen, C., Assmy, P., Falk-Petersen, S., Kohler, J., Kovacs, K. M., Reigstad, M., Steen, H.,
737 Strøm, H., Sundfjord, A., Varpe, Ø., Walczowski, W., Weslawski, J. M. and Zajaczkowski, M.:
738 The importance of tidewater glaciers for marine mammals and seabirds in Svalbard, Norway, *J.*
739 *Mar. Syst.*, 129, 452–471, doi:10.1016/j.jmarsys.2013.09.006, 2014.

740 Maar, M., Møller, E. F., Larsen, J., Madsen, K. S., Wan, Z., She, J., Jonasson, L. and Neumann,
741 T.: Ecosystem modelling across a salinity gradient from the North Sea to the Baltic Sea, *Ecol.*
742 *Modell.*, 222(10), 1696–1711, doi:10.1016/j.ecolmodel.2011.03.006, 2011.

743 Maar, M., Markager, S., Madsen, K. S., Windolf, J., Lyngsgaard, M. M., Andersen, H. E. and
744 Møller, E. F.: The importance of local versus external nutrient loads for Chl a and primary
745 production in the Western Baltic Sea, *Ecol. Modell.*, 320, doi:10.1016/j.ecolmodel.2015.09.023,
746 2016.

747 Maar, M. Møller, E.F., Larsen J. (2022). FlexSem Biogeochemical model for Disko Bay,
748 Greenland. (Version v16). Zenodo. <https://doi.org/10.5281/zenodo.7401870>

749 Madsen, K. S., Rasmussen, T. A. S., Ribergaard, M. H. and Ringgaard, I. M.: High resolution
750 sea-ice modelling and validation of the Arctic with focus on South Greenland Waters, 2004-
751 2013, *Polarforschung*, 85(2), 101–105, doi:10.2312/polfor.2016.006, 2016.

752 Mankoff, K. D., Straneo, F., Cenedese, C., Das, S. B., Richards, C. G. and Singh, H.: Structure
753 and dynamics of a subglacial discharge plume in a <sc>G</sc> reenlandic fjord, *J. Geophys.*
754 *Res. Ocean.*, 121(12), 8670–8688, doi:10.1002/2016JC011764, 2016.

755 Mankoff, K. D., Solgaard, A., Colgan, W., Ahlstrøm, A. P., Abbas Khan, S. and Fausto, R. S.:
756 Greenland Ice Sheet solid ice discharge from 1986 through March 2020, *Earth Syst. Sci. Data*,
757 12(2), 1367–1383, doi:10.5194/essd-12-1367-2020, 2020a.

758 Mankoff, K. D., Ahlstrøm, A. P., Colgan, W., Faust, R. S., Fettweis, X., Kondo, K., Langley, K.,
759 Noël, B., Sugiyama, S. and As, D. van: Greenland liquid water runoff from 1979 through 2017,
760 *Earth Syst. Sci. Data*, (April), doi:doi.org/10.5194/essd-2020-47, 2020b.

761 Mankoff, K. D., Fettweis, X., Langen, P. L., Stendel, M., Kjeldsen, K. K., Karlsson, N. B., Noël,
762 B., van den Broeke, M. R., Solgaard, A., Colgan, W., Box, J. E., Simonsen, S. B., King, M. D.,
763 Ahlstrøm, A. P., Andersen, S. B. and Fausto, R. S.: Greenland ice sheet mass balance from 1840
764 through next week, *Earth Syst. Sci. Data*, 13(10), 5001–5025, doi:10.5194/essd-13-5001-2021,
765 2021.

766 Massicotte, P., Peeken, I., Katlein, C., Flores, H., Huot, Y., Castellani, G., Arndt, S., Lange, B.
767 A., Tremblay, J.-É. and Babin, M.: Sensitivity of phytoplankton primary production estimates to
768 available irradiance under heterogeneous sea-ice conditions, *J. Geophys. Res. Ocean.*, (June),
769 doi:10.1029/2019JC015007, 2019.

770 Meier, W. N., Hovelsrud, G. K., van Oort, B. E. H., Key, J. R., Kovacs, K. M., Michel, C., Haas,
771 C., Granskog, M. A., Gerland, S., Perovich, D. K., Makshtas, A. and Reist, J. D.: Arctic sea ice
772 in transformation: A review of recent observed changes and impacts on biology and human
773 activity, *Rev. Geophys.*, 52(3), 185–217, doi:10.1002/2013RG000431, 2014.

774 Meire, L., Mortensen, J., Meire, P., Juul-Pedersen, T., Sejr, M. K., Rysgaard, S., Nygaard, R.,

775 Huybrechts, P. and Meysman, F. J. R.: Marine-terminating glaciers sustain high productivity in
776 Greenland fjords, *Glob. Chang. Biol.*, 23(12), 5344–5357, doi:10.1111/gcb.13801, 2017.

777 Menden-Deuer, S., Lawrence, C. and Franzè, G.: Herbivorous protist growth and grazing rates at
778 in situ and artificially elevated temperatures during an Arctic phytoplankton spring bloom, *PeerJ*,
779 2018(7), doi:10.7717/peerj.5264, 2018.

780 Møller, E. F. and Nielsen, T. G.: Borealization of Arctic zooplankton — smaller and less fat
781 zooplankton species in Disko Bay , Western Greenland, , 1–14, doi:10.1002/lno.11380, 2019.

782 Møller, E. F. and Nielsen, T. G.: Borealization of Arctic zooplankton—smaller and less fat
783 zooplankton species in Disko Bay, Western Greenland, *Limnol. Oceanogr.*, 65(6), 1175–1188,
784 doi:10.1002/lno.11380, 2020.

785 Møller, E. F. E. F., Maar, M., Jónasdóttir, S. H. S. H., Gissel Nielsen, T. and Tönnesson, K.: The
786 effect of changes in temperature and food on the development of *Calanus finmarchicus* and
787 *Calanus helgolandicus* populations, *Limnol. Oceanogr.*, 57(1), 211–220,
788 doi:10.4319/lo.2012.57.1.0211, 2012.

789 Møller, E. F. E. F., Bohr, M., Kjellerup, S., Maar, M., Møhl, M., Swalethorp, R. and Nielsen, T.
790 G. T. G.: *Calanus finmarchicus* egg production at its northern border, *J. Plankton Res.*, 38(5),
791 1206–1214, doi:10.1093/plankt/fbw048, 2016.

792 Møller, E.F., Nielsen, T.G. (2022). Borealization of Arctic zooplankton—smaller and less fat
793 zooplankton species in Disko Bay, Western Greenland [Data set]. Zenodo.
794 <https://doi.org/10.5281/zenodo.745457>

795 Møller, E.F., Christensen, A., Larsen, J, Mankoff, K. D., Ribergaard, M. H., Sejr, M. K.,
796 Wallhead, P., Maar, M (2022). The sensitivity of primary productivity in Disko Bay, a coastal
797 Arctic ecosystem to changes in freshwater discharge and sea ice cover [Data set]. Zenodo.
798 <https://doi.org/10.5281/zenodo.7454727>

799 Morlighem, M., Williams, C. N., Rignot, E., An, L., Arndt, J. E., Bamber, J. L., Catania, G.,
800 Chauché, N., Dowdeswell, J. A., Dorschel, B., Fenty, I., Hogan, K., Howat, I., Hubbard, A.,
801 Jakobsson, M., Jordan, T. M., Kjeldsen, K. K., Millan, R., Mayer, L., Mouginot, J., Noël, B. P.
802 Y., O’Cofaigh, C., Palmer, S., Rysgaard, S., Seroussi, H., Siegert, M. J., Slabon, P., Straneo, F.,

803 van den Broeke, M. R., Weinrebe, W., Wood, M. and Zinglensen, K. B.: BedMachine v3:
804 Complete Bed Topography and Ocean Bathymetry Mapping of Greenland From Multibeam
805 Echo Sounding Combined With Mass Conservation, *Geophys. Res. Lett.*, 44(21), 11,051-11,061,
806 doi:10.1002/2017GL074954, 2017.

807 Mortensen, J., Rysgaard, S., Bendtsen, J., Lennert, K., Kanzow, T., Lund, H. and Meire, L.:
808 Subglacial Discharge and Its Down-Fjord Transformation in West Greenland Fjords With an Ice
809 Mélange, *J. Geophys. Res. Ocean.*, 125(9), 1–13, doi:10.1029/2020JC016301, 2020.

810 Mouginot, J., Rignot, E., Bjørk, A. A., van den Broeke, M., Millan, R., Morlighem, M., Noël, B.,
811 Scheuchl, B. and Wood, M.: Forty-six years of Greenland Ice Sheet mass balance from 1972 to
812 2018, *Proc. Natl. Acad. Sci. U. S. A.*, 116(19), 9239–9244, doi:10.1073/pnas.1904242116, 2019.

813 Murray, C., Markager, S., Stedmon, C. A., Juul-Pedersen, T., Sejr, M. K. and Bruhn, A.: The
814 influence of glacial melt water on bio-optical properties in two contrasting Greenlandic fjords,
815 *Estuar. Coast. Shelf Sci.*, 163(PB), 72–83, doi:10.1016/j.ecss.2015.05.041, 2015.

816 Neumann, T.: Towards a 3D-ecosystem model of the Baltic Sea, *J. Mar. Syst.*, 25(3–4), 405–
817 419, doi:10.1016/S0924-7963(00)00030-0, 2000.

818 Pabi, S., van Dijken, G. L. and Arrigo, K. R.: Primary production in the Arctic Ocean, 1998-
819 2006, *J. Geophys. Res. Ocean.*, 113(8), 1998–2006, doi:10.1029/2007JC004578, 2008.

820 Randelhoff, A., Holding, J., Janout, M., Sejr, M. K., Babin, M., Tremblay, J.-éric, Alkire, M. B.
821 and Oliver, H.: Pan-Arctic Ocean Primary Production Constrained by Turbulent Nitrate Fluxes, ,
822 7(March), 1–15, doi:10.3389/fmars.2020.00150, 2020.

823 Rasmussen, T. A. S., Høyer, J. L., Ghent, D., Bulgin, C. E., Dybkjær, G., Ribergaard, M. H.,
824 Nielsen-Englyst, P. and Madsen, K. S.: Impact of Assimilation of Sea-Ice Surface Temperatures
825 on a Coupled Ocean and Sea-Ice Model, *J. Geophys. Res. Ocean.*, 123(4), 2440–2460,
826 doi:10.1002/2017JC013481, 2018.

827 Ross, O. N. and Geider, R. J.: New cell-based model of photosynthesis and photo-acclimation:
828 accumulation and mobilisation of energy reserves in phytoplankton, *Mar. Ecol. Prog. Ser.*, 383,
829 53–71, doi:10.3354/meps07961, 2009.

830 Rysgaard, S., Boone, W., Carlson, D., Sejr, M. K., Bendtsen, J., Juul-Pedersen, T., Lund, H.,

831 Meire, L. and Mortensen, J.: An Updated View on Water Masses on the pan-West Greenland
832 Continental Shelf and Their Link to Proglacial Fjords, *J. Geophys. Res. Ocean.*, 125(2), 0–3,
833 doi:10.1029/2019JC015564, 2020.

834 Sejr, M. K., Nielsen, T. G., Rysgaard, S., Risgaard-petersen, N., Sturluson, M. and Blicher, M.
835 E.: Fate of pelagic organic carbon and importance of pelagic – benthic coupling in a shallow
836 cove, *Mar. Ecol. Prog. Ser.*, 341, 75–88, 2007.

837 Shchepetkin, A. F. and McWilliams, J. C.: The regional oceanic modeling system (ROMS): A
838 split-explicit, free-surface, topography-following-coordinate oceanic model, *Ocean Model.*, 9(4),
839 347–404, doi:10.1016/j.ocemod.2004.08.002, 2005.

840 Steele, M., Morley, R. and Ermold, W.: PHC: A global ocean hydrography with a high-quality
841 Arctic Ocean, *J. Clim.*, 14(9), 2079–2087, doi:10.1175/1520-
842 0442(2001)014<2079:PAGOHW>2.0.CO;2, 2001.

843 Stroeve, J. C., Markus, T., Boisvert, L., Miller, J. and Barrett, A.: Changes in Arctic melt season
844 and implications for sea ice loss, *Geophys. Res. Lett.*, 41(4), 1216–1225,
845 doi:10.1002/2013GL058951, 2014.

846 Swalethorp, R., Kjellerup, S., Dünweber, M., Nielsen, T., Møller, E., Rysgaard, S. and Hansen,
847 B.: Grazing, egg production, and biochemical evidence of differences in the life strategies of
848 *Calanus finmarchicus*, *C. glacialis* and *C. hyperboreus* in Disko Bay, western Greenland, *Mar.*
849 *Ecol. Prog. Ser.*, 429, 125–144, doi:10.3354/meps09065, 2011.

850 Thomas, D. N., Baumann, M. E. M. and Gleitz, M.: Efficiency of carbon assimilation and
851 photoacclimation in a small unicellular *Chaetoceros* species from the Weddell Sea (Antarctica):
852 influence of temperature and irradiance, *J. Exp. Mar. Bio. Ecol.*, 157(2), 195–209,
853 doi:10.1016/0022-0981(92)90162-4, 1992.

854 Thyrring, J., Wegeberg, S., Blicher, M. E., Krause-Jensen, D., Høgslund, S., Olesen, B., Jozef,
855 W., Mouritsen, K. N., Peck, L. S. and Sejr, M. K.: Latitudinal patterns in intertidal ecosystem
856 structure in West Greenland suggest resilience to climate change, *Ecography (Cop.)*, 44(8),
857 1156–1168, doi:10.1111/ecog.05381, 2021.

858 Tremblay, J.-É. and Gagnon, J.: The effects of irradiance and nutrient supply on the productivity

859 of Arctic waters: a perspective on climate change, in *Influence of Climate Change on the*
860 *Changing Arctic and Sub-Arctic Conditions*, pp. 73–93, Springer Netherlands, Dordrecht., 2009.

861 Tremblay, J. É., Anderson, L. G., Matrai, P., Coupel, P., Bélanger, S., Michel, C. and Reigstad,
862 M.: Global and regional drivers of nutrient supply, primary production and CO₂ drawdown in
863 the changing Arctic Ocean, *Prog. Oceanogr.*, 139, 171–196, doi:10.1016/j.pocean.2015.08.009,
864 2015.

865 Vernet, M., Ellingsen, I., Marchese, C., Bélanger, S., Cape, M., Slagstad, D. and Matrai, P. A.:
866 Spatial variability in rates of Net Primary Production (NPP) and onset of the spring bloom in
867 Greenland shelf waters, *Prog. Oceanogr.*, 198(September 2020), 102655,
868 doi:10.1016/j.pocean.2021.102655, 2021.

869 Yang, X., Petersen, C., Amstrup B., Andersen, B. S., Hansen, Feddersen, H., Kmit, M.,
870 Korsholm, U., Lindberg, K., Mogensen, K., Sass, B.H., Sattler, K., Nielsen, N.W.: The DMI-
871 HIRLAM upgrade in June 2004. DMI-Tech. Rep. 05-09, Danish Meteorological Institute,
872 Copenhagen, Denmark, 2005.

873 Yang, X., Palmason, B., Andersen, B. S., Hansen Sass, B., Amstrup, B., Dahlbom, M., Petersen,
874 C., Pagh Nielsen, K., Mottram, R., Woetmann, N., Mahura, A. Thorsteinsson, S., Nawri, N., and
875 Petersen, G. N. 2017: IGA, the Joint Operational HARMONIE by DMI and IMO, ALADIN-
876 HIRLAM Newsletter, No. 8, 87–94, 2017.

877 Yang, X., Palmason, B., Sattler, K., Thorsteinsson, S., Amstrup, B., Dahlbom, M, Hansen Sass,
878 B., Pagh Nielsen, K., Petersen, G. N. 2018: IGB, the Upgrade to the Joint Operational
879 HARMONIE by DMI and IMO in 2018, ALADIN-HIRLAM Newsletter, No. 11, 93-96, 2018.

880 Zhang, J., Spitz, Y. H., Steele, M., Ashjian, C., Campbell, R., Berline, L. and Matrai, P.:
881 Modeling the impact of declining sea ice on the Arctic marine planktonic ecosystem, *J. Geophys.*
882 *Res. Ocean.*, 115(10), doi:10.1029/2009JC005387, 2010.

883

884

885 9 Tables

886 Table 1: Characteristics of the reference model runs of 2010 and 2017, and the annual average
 887 NPP in the bay obtained from scenarios runs with changes in the sea ice cover and the freshwater
 888 discharge (Figure 8 and 9). SD are the standard variation between the different model grid cells.

				2010	2017
Reference	Average annual primary production	gC m ⁻² yr ⁻¹		147 ±41	90 ±28
	Average annual discharge	m ³ s ⁻¹		6275	4058
	Average annual sea ice cover, March-April	%		24	79
Scenarios	Average annual primary production	gC m ⁻² yr ⁻¹	No sea ice	150 ±50	120 ±35
			No freshwater discharge	144 ±53	90 ±46
			No sea ice, No freshwater discharge	147 ±47	119 ±32
			2 x freshwater discharge	149 ±48	90 ±45
			No sea ice, 2 x freshwater discharge	152 ±53	122 ±35

889

890 Table 2: Statistics for seasonal comparison between observational data (monthly climatology)
 891 and model data (monthly average from 2005 to 2018) at the Disko Bay Station. $N=12$ for
 892 copepods, $N=11$ for temperature, salinity and Chl *a* and $N=10$ for other variables (see Figure 4).
 893 All correlations were significant ($p<0.01$).

894

	Unit	Model error	RMSE	Correlat ion	<i>cf</i>
Temperature	°C	-0.28	0.96	0.94	0.31
Salinity	-	-0.09	0.21	0.79	0.56
NO ₃	mmol m ⁻³	0.00	1.43	0.87	0.39
Silicate	mmol m ⁻³	0.78	1.70	0.83	0.66
Phosphate	mmol m ⁻³	-0.01	0.12	0.82	0.46
<i>Chl a</i>	mg m ⁻³	0.03	0.97	0.87	0.37
Copepod biomass	mgC m ⁻³	0.83	4.66	0.94	0.23

895

896 Table 3: Statistics for the spatial comparison between remote sensing data and surface model
 897 data for spring (April-June) and summer (July-September) in 2010 and 2017. In spring 2017,
 898 only June is included due to ice cover in April-May. $N=6145$, and all correlations were
 899 significant ($p<0.01$).

	Model error	RMSE	Correlatio n	<i>cf</i>
<i>Surface temperature</i>				
2010 spring	0.8	1.3	0.45	1.0
2010 summer	-1.4	2.0	0.14	1.5
2017 spring	0.8	1.4	0.58	0.9
2017 summer	-2.0	2.3	0.33	0.2
<i>Log₁₀ (Chl a [mg/m³])</i>				
2010 spring	0.6	0.7	0.30	0.4
2010 summer	0.5	0.8	0.33	0.2
2017 spring	1.7	1.8	0.29	1.7
2017 summer	0.9	1.1	0.46	1.2

900

901 10 Figures

902 Figure 1: Map of Disko Bay with the bathymetry, the Flexsem model grid, position of
903 freshwater sources (red dots: land runoff, red dots with black circle: land + ice runoff), position
904 of two stations presented in more detail, and the area used for calculation of the average Disko
905 Bay primary production (red box).

906 Figure 2: Development in freshwater discharge and sea ice cover over time. a) Freshwater
907 discharge from the Greenland ice sheet divided into liquid from precipitation over land (Land
908 runoff), liquid deriving from melt from the Greenland Ice sheet/glaciers (Ice runoff) and ice
909 deriving directly from the glacier (solid ice) 1960 to 2019, and b) number of days with more than
910 40% sea ice cover from 1986 to 2019, derived from satellite measurement (AICE), by the sea ice
911 model providing input to the this study (CICE), and by visual observation at Arctic Station,
912 Qeqertarsuaq (AS).

913 Figure 3: Primary production, sea ice cover and freshwater discharge in Disko Bay from 2004 to
914 2018. Primary production and sea ice cover are assessed in the red square in Fig 1, whereas the
915 freshwater discharge are from the full model domain. (a) Average annual primary production (gC
916 $\text{m}^{-2} \text{year}^{-1}$) \pm SD (variation between model grid cells), (b) the average monthly primary
917 production ($\text{mgC m}^{-2} \text{day}^{-1}$) \pm SD (variation between years), light is average from Arctic station
918 (2010-2019), (c) the annual average sea ice cover in March and April (%), (d) the average
919 monthly sea ice cover (%), (e) the average annual freshwater discharge ($\text{m}^3 \text{s}^{-1}$), and (f) the
920 average monthly freshwater discharge ($1000 \text{m}^3 \text{s}^{-1}$).

921 Figure 4: Comparison of monthly means (\pm SD) of observations and model data (2004-2018) at
922 $69^{\circ}14' \text{N}$, $53^{\circ}23' \text{W}$ for (a) temperature ($^{\circ}\text{C}$), (b) salinity, (c) nitrate (mmol m^{-3}), (d) silicate
923 (mmol m^{-3}), (e) phosphate (mmol m^{-3}), (f) Chl *a*, (mg m^{-3}), (g) microzooplankton biomass (mgC
924 m^{-3}), and (h) mesozooplankton biomass (mgC m^{-3}). Means are averaged over 0-20 m depth,
925 except for mesozooplankton which it is 0-50 m.

926 Figure 5: Sea ice cover (%), average nitrate concentration in 0-30 m (mmol m^{-3}) average Chl *a*
927 concentration in 0-30 m (mg m^{-3}) and primary production ($\text{mgC m}^{-2} \text{d}^{-1}$) at a station in open Bay
928 (Bay Station) and at one close to the glacier (Glacier Station) (Fig. 1) in 2010 and 2017.

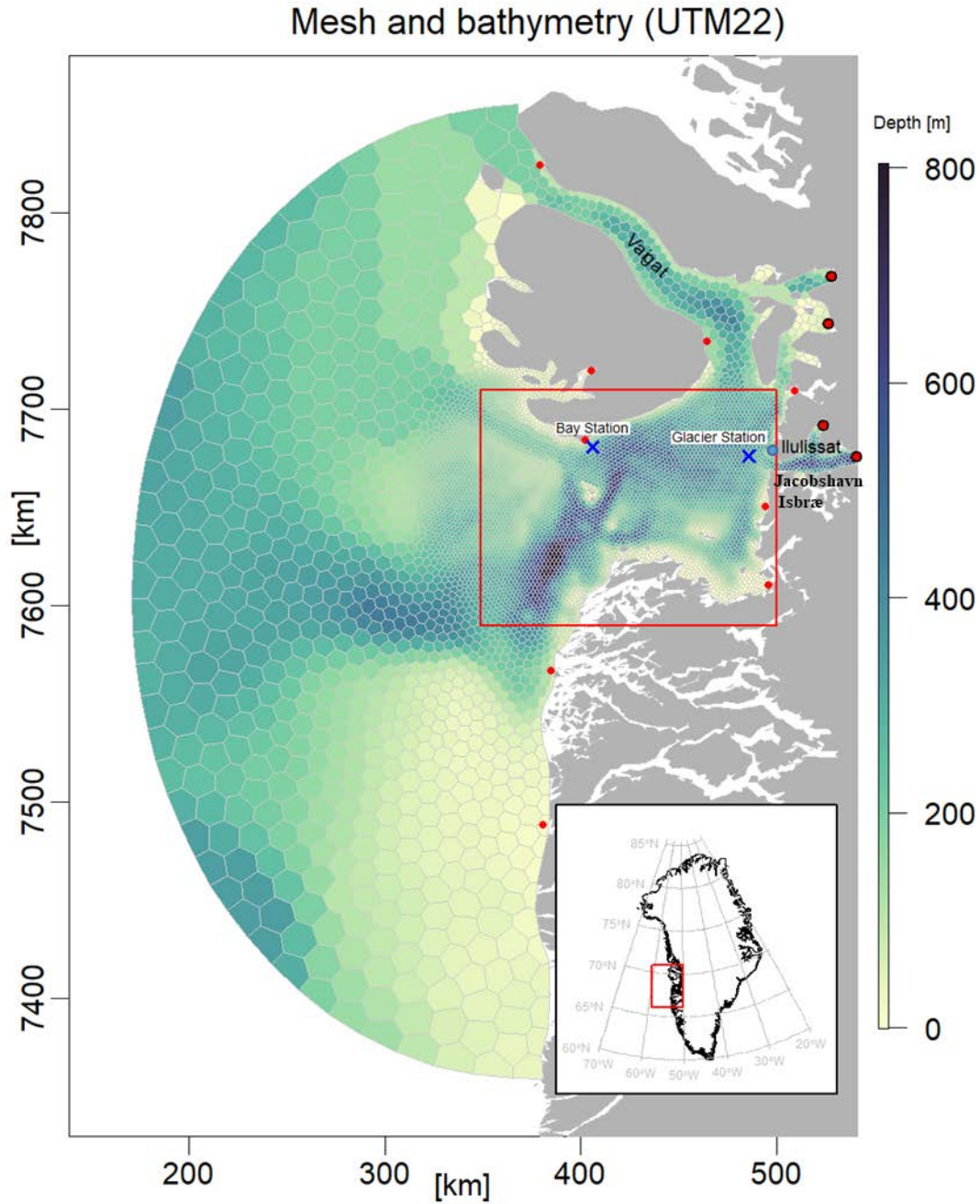
929 Figure 6: Average spatial distribution of primary production (gC m^{-2}) in 2010 and 2017
930 respectively for the periods A)+D) March-October, B)+E) March-June and C) +F) July-October.

931 Figure 7: Correlation coefficients between the annual primary production (a) and average sea ice
932 cover in March-April and (b) and surface salinity across the period 2004-2018.

933 Figure 8: Response of the annual primary production to simple scenarios of changes in sea ice
934 cover and freshwater discharge (Q) in 2010 expressed as percentage change relative to the
935 standard model run. The percentages in the bottom of the figure are the changes in primary
936 production in the total area shown. The following model scenarios were run (Table 1): (a)
937 standard model run, (b) assuming no sea ice cover, (c) assuming no freshwater discharge from
938 the Greenland ice sheet, (d) the combination of (b) and (c), (e) assuming 2 times the freshwater
939 discharge of the standard run, and (f) the combination of (b) and (e).

940 Figure 9: Response of the annual primary production to simple scenarios of changes in sea ice
941 cover and freshwater discharge (Q) in 2017 expressed as percentage change relative to the
942 standard model run. The percentages in the bottom of the figure are the changes in primary
943 production in the total area shown. The following model scenarios were run (Table 1): (a)
944 standard model run, (b) assuming no sea ice cover, (c) assuming no freshwater discharge from
945 the Greenland ice sheet, (d) the combination of (b) and (c), (e) assuming 2 times the freshwater
946 discharge of the standard run, and (f) the combination of (b) and (e).

Figure 1: Map of Disko Bay with the bathymetry, the Flexsem model grid, position of freshwater sources (red dots: land runoff, red dots with black circle: land + ice runoff), position of two stations presented in more detail, and the area used for calculation of the average Disko Bay primary production (red box).



947
948

Figure 2: Development in freshwater discharge and sea ice cover over time. a) Freshwater discharge from the Greenland ice sheet divided into liquid from precipitation over land (Land runoff), liquid deriving from melt from the Greenland Ice sheet/glaciers (Ice runoff) and ice deriving directly from the glacier (solid ice) 1960 to 2019, and b) number of days with more than 40% sea ice cover from 1986 to 2019, derived from satellite measurement (AICE), by the sea ice model providing input to the this study (CICE), and by visual observation at Arctic Station, Qeqertarsuaq (AS).

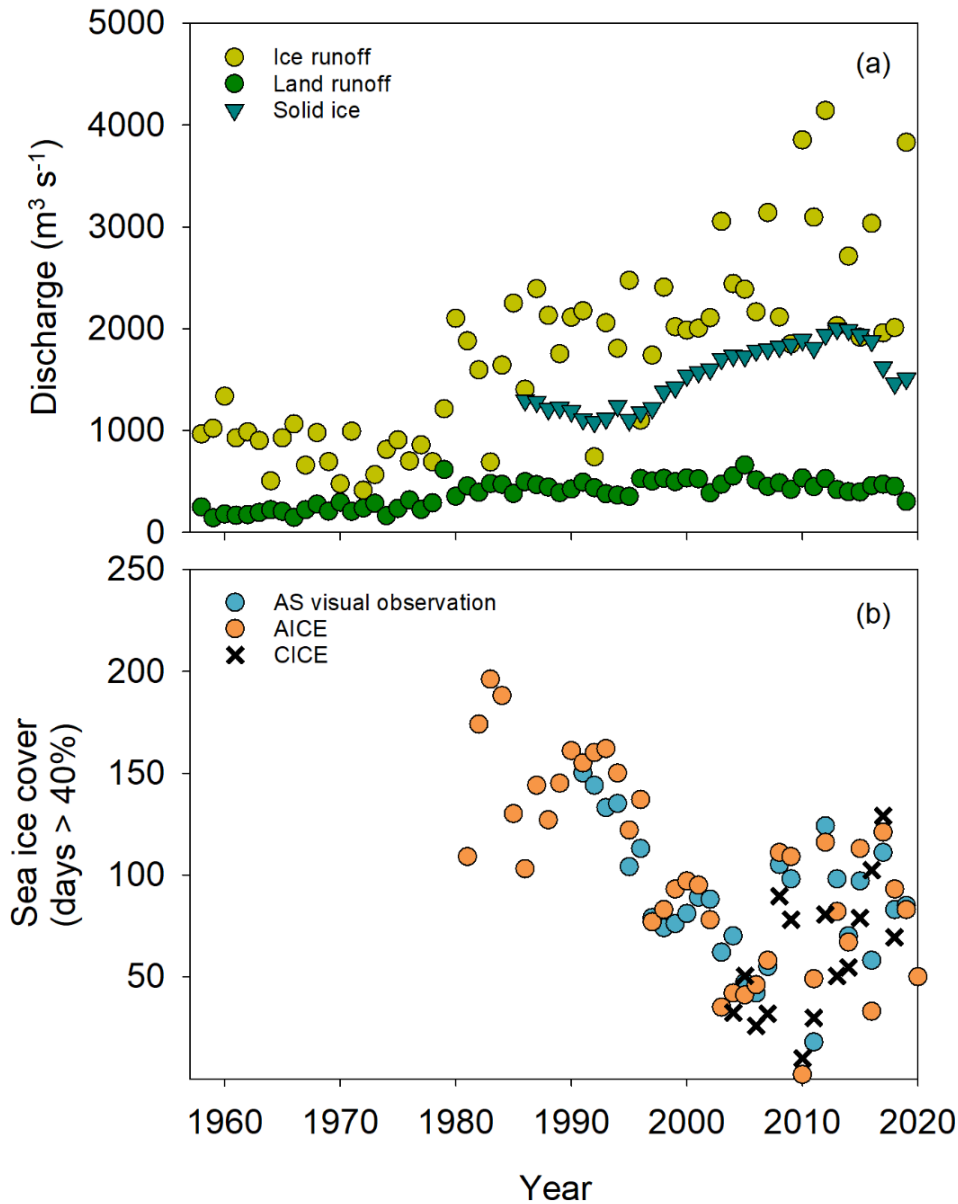


Figure 3: Primary production, sea ice cover and freshwater discharge in Disko Bay from 2004 to 2018. Primary production and sea ice cover are assessed in the red square in Fig 1, whereas the freshwater discharge are from the full model domain. (a) Average annual primary production ($\text{gC m}^{-2} \text{ year}^{-1}$) \pm SD (variation between model grid cells), (b) the average monthly primary production ($\text{mgC m}^{-2} \text{ day}^{-1}$) \pm SD (variation between years), light is average from Arctic station (2010-2019), (c) the annual average sea ice cover in March and April (%), (d) the average monthly sea ice cover (%), (e) the average annual freshwater discharge ($\text{m}^3 \text{ s}^{-1}$), and (f) the average monthly freshwater discharge ($1000 \text{ m}^3 \text{ s}^{-1}$).

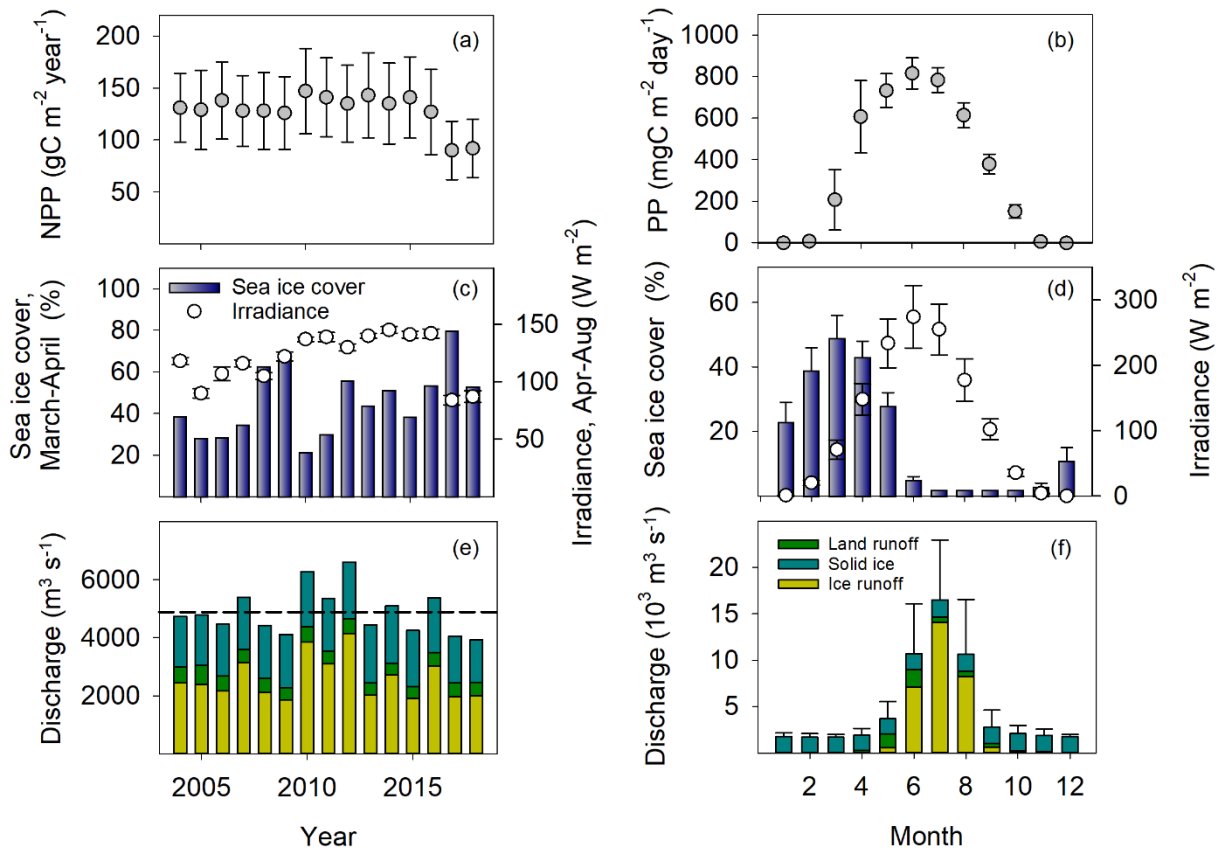
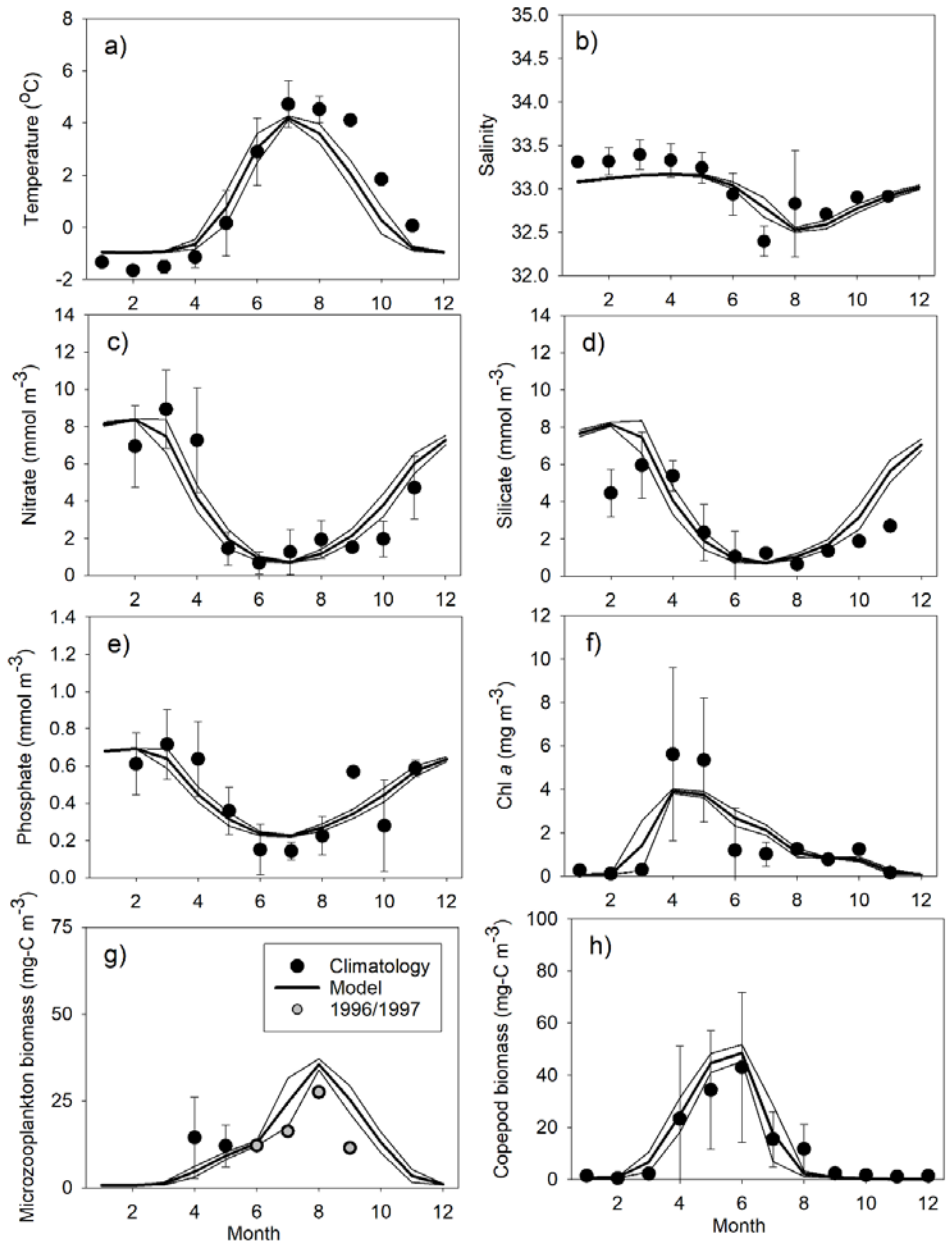


Figure 4: Comparison of monthly means (\pm SD) of observations and model data (2004-2018) at $69^{\circ}14'N$, $53^{\circ}23'W$ for (a) temperature ($^{\circ}C$), (b) salinity, (c) nitrate ($mmol\ m^{-3}$), (d) silicate ($mmol\ m^{-3}$), (e) phosphate ($mmol\ m^{-3}$), (f) Chl *a*, ($mg\ m^{-3}$), (g) microzooplankton biomass ($mgC\ m^{-3}$), and (h) mesozooplankton biomass ($mgC\ m^{-3}$). Means are averaged over 0-20 m depth, except for mesozooplankton which it is 0-50 m.



951

952

Fig 5: Sea ice cover (%), average nitrate concentration in 0-30 m (mmol m^{-3}) average Chl *a* concentration in 0-30 m (mg m^{-3}) and primary production ($\text{mgC m}^{-2} \text{d}^{-1}$) at a station in open Bay (Bay Station) and at one close to the glacier (Glacier Station) (Fig. 1) in 2010 and 2017.

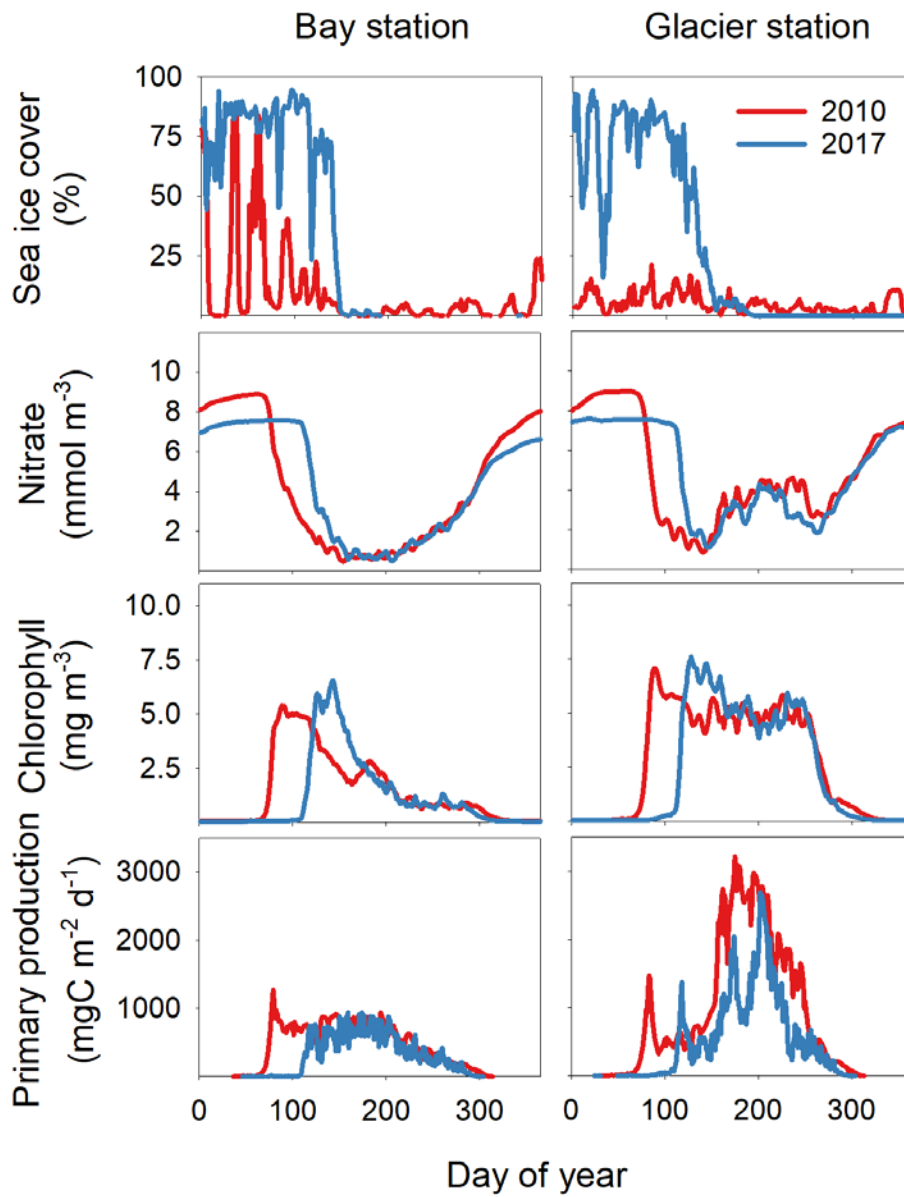


Fig 6: Average spatial distribution of primary production (gC m^{-2}) in 2010 and 2017 respectively for the periods A)+D) March-October, B)+E) March-June and C) +F) July-October.

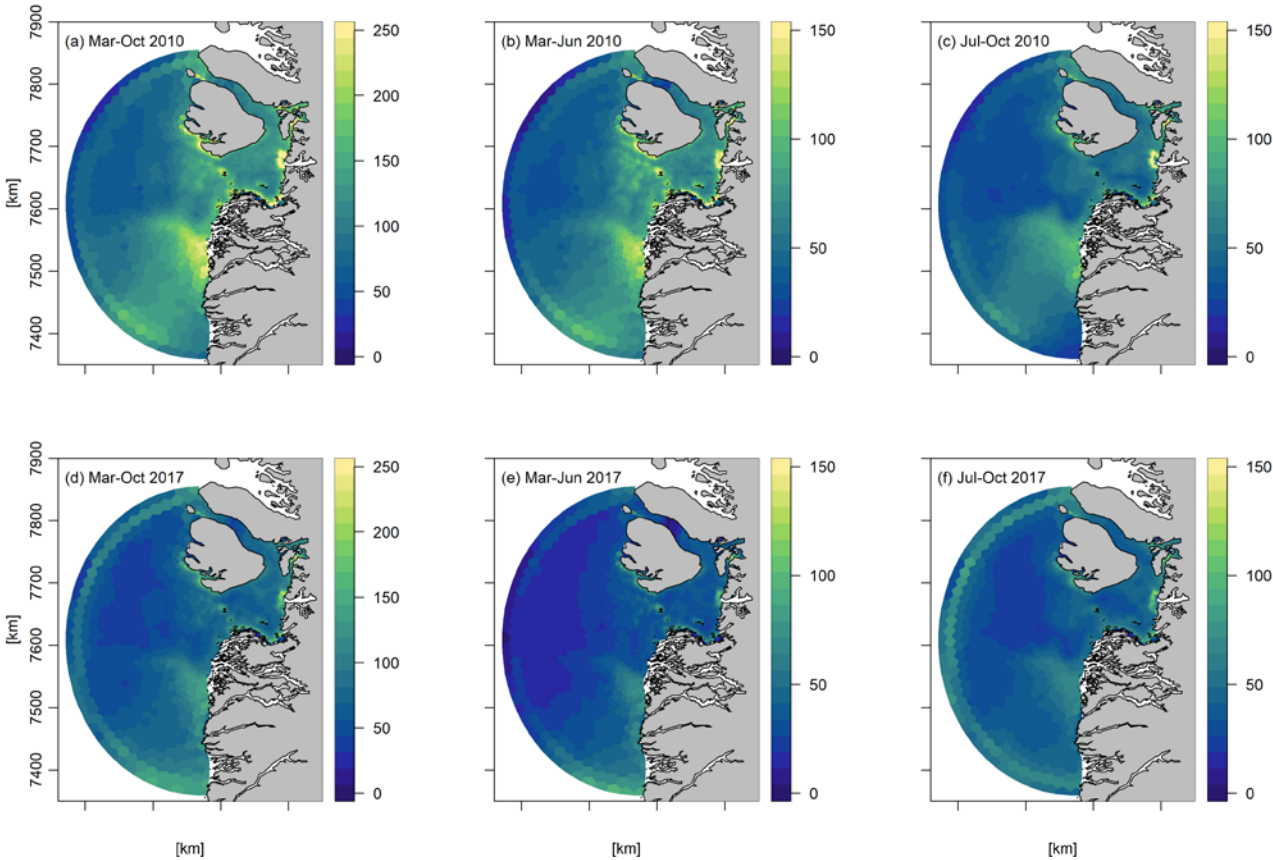


Fig 7: Correlation coefficients between the annual primary production (a) and average sea ice cover in March-April and (b) and surface salinity across the period 2004-2018.

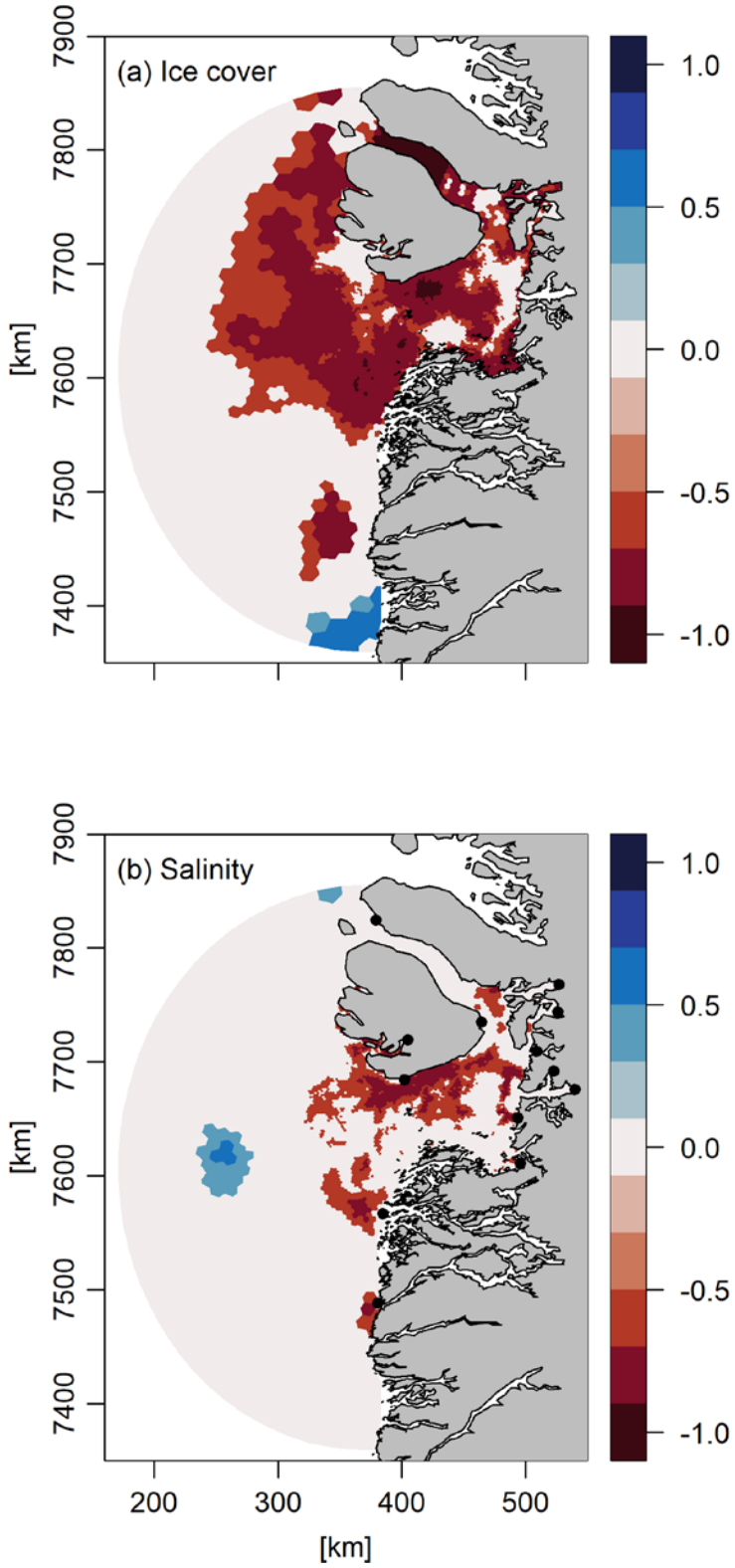


Fig 8: Response of the annual primary production to simple scenarios of changes in sea ice cover and freshwater discharge (Q) in 2010 expressed as percentage change relative to the standard model run. The percentages in the bottom of the figure are the changes in primary production in the total area shown. The following model scenarios were run (Table 1): (a) standard model run, (b) assuming no sea ice cover, (c) assuming no freshwater discharge from the Greenland ice sheet, (d) the combination of (b) and (c), (e) assuming 2 times the freshwater discharge of the standard run, and (f) the combination of (b) and (e).

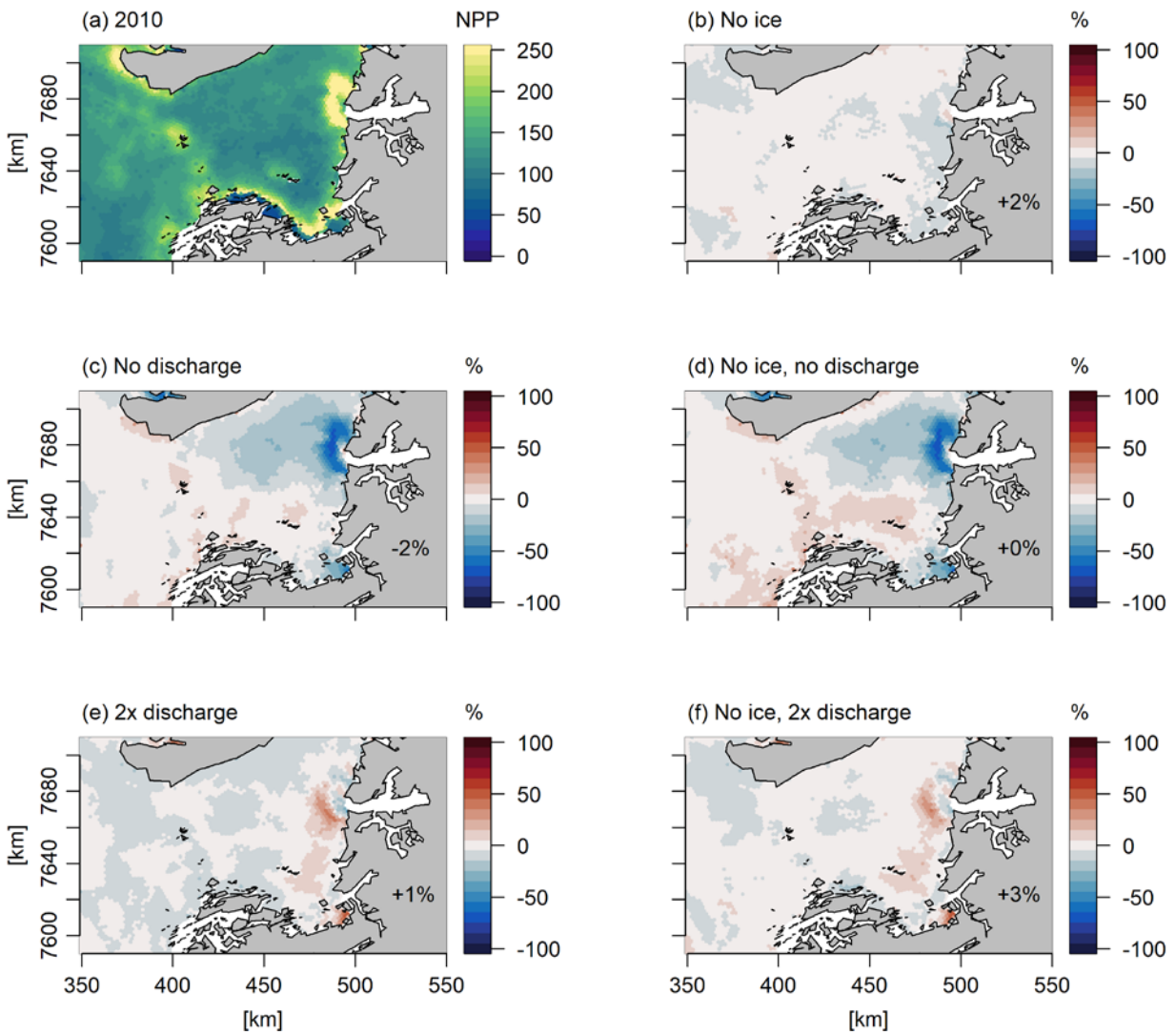
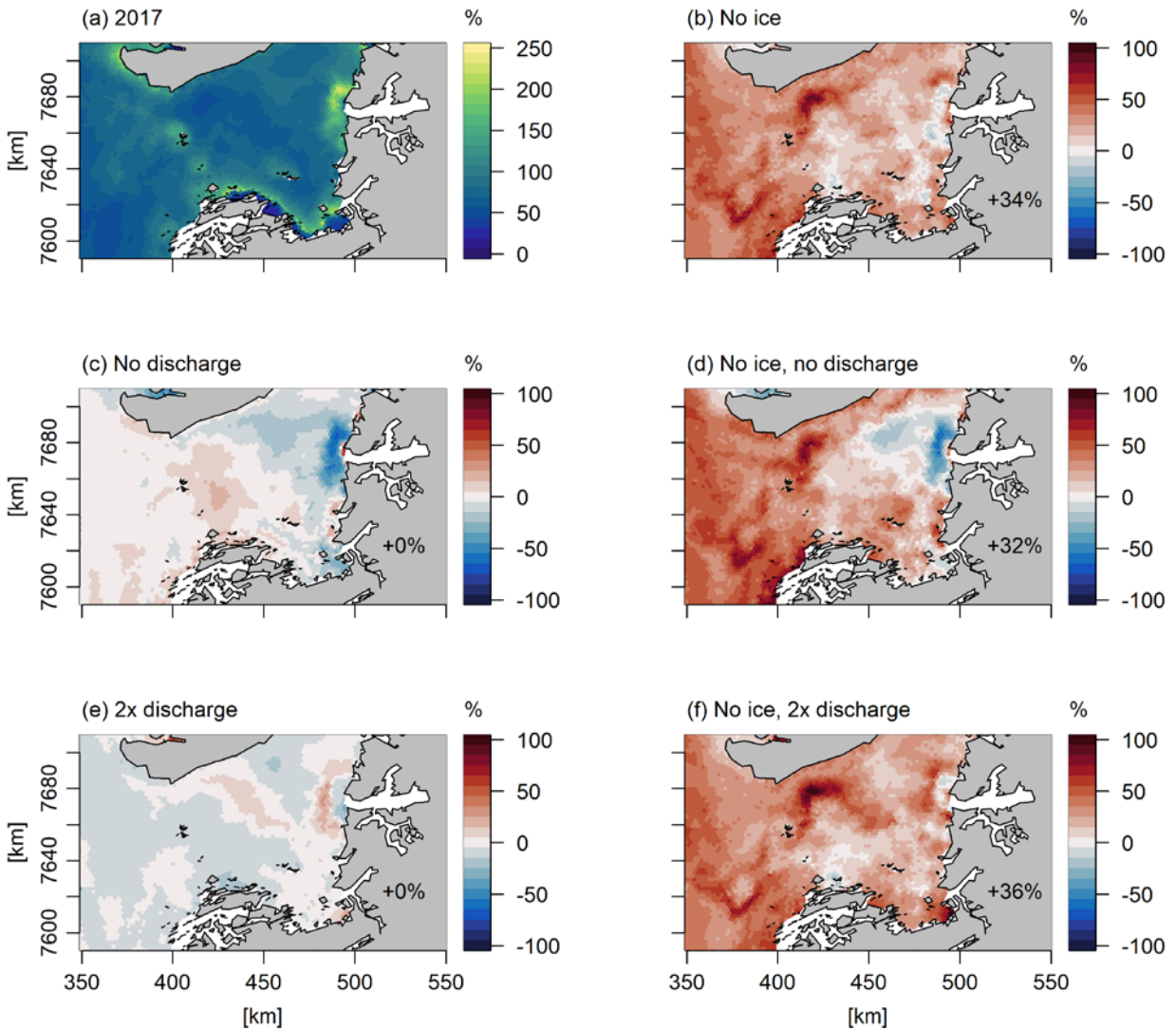


Fig 9: Response of the annual primary production to simple scenarios of changes in sea ice cover and freshwater discharge (Q) in 2017 expressed as percentage change relative to the standard model run. The percentages in the bottom of the figure are the changes in primary production in the total area shown. The following model scenarios were run (Table 1): (a) standard model run, (b) assuming no sea ice cover, (c) assuming no freshwater discharge from the Greenland ice sheet, (d) the combination of (b) and (c), (e) assuming 2 times the freshwater discharge of the standard run, and (f) the combination of (b) and (e).



957 11 Appendices

958 11.1 Appendix A, Ecological model constants

959 Table A.1. Constants in the FlexSem ecological Disko Bay model.

Parameter	Description	Numerical value	Units
Phytoplankton			
α_1	Half-saturation uptake diatoms	0.55	mmol-N m ⁻³
α_2	Half-saturation uptake flagellates	0.45	mmol-N m ⁻³
RD_0	Maximum uptake diatoms at 0°C	1.50	d ⁻¹
RF_0	Maximum uptake flagellates at 0°C	0.75	d ⁻¹
S_{DIA}	Sinking rate diatoms	-1	m d ⁻¹
$Iopt_{dia}$	Optimum PAR diatoms	95	W m ⁻²
$Iopt_{flag}$	Optimum PAR flagellates	105	W m ⁻²
k_c	Attenuation constant self-shading	0.03	m ² (mg Chl a) ⁻¹
LPN	Loss rate phytoplankton to nutrients at 0°C	0.03	d ⁻¹
LPD	Loss rate phytoplankton to detritus at 0°C	0.02	d ⁻¹
Ths_1	Half-saturation temperature diatoms	12	°C
Ths_2	Half-saturation temperature flagellates	7	°C
Q_{10}	Maintenance temperature coefficient	0.07	°C ⁻¹
RFR	Redfield ratio N:P (mol-based)	16:1	fraction
N:Si	Si:N-ratio (mol-based)	1.1	fraction
Zooplankton			
$Imax_{MEZ}$	Maximum grazing mesozooplankton at 12°C	0.47	d ⁻¹
$Imax_{MIZ}$	Maximum grazing microzooplankton at 0°C	0.60	d ⁻¹
K_{MEZ}	Half-saturation ingestion mesozooplankton	0.32	mmol-N m ⁻³
K_{MIZ}	Half-saturation ingestion microzooplankton	0.60	mmol-N m ⁻³
AE_{MEZ}	Assimilation efficiency mesozooplankton	0.65	fraction
AE_{MIZ}	Assimilation efficiency microzooplankton	0.60	fraction
R_{MEZ}	Active respiration mesozooplankton	0.29	fraction
R_{MIZ}	Active respiration microzooplankton	0.35	fraction
β_{MEZ}	Basal respiration mesozooplankton at 0°C	0.005	d ⁻¹
β_{MIZ}	Basal respiration microzooplankton at 0°C	0.03	d ⁻¹
$pref_{DI}$	Grazing preference for diatoms by MEZ and MIZ	1.0	fraction
$pref_{FL}$	Grazing preference for flagellates by MEZ and MIZ	1.0	fraction
$pref_{MIZ}$	Grazing preference for microzooplankton by MEZ	1.0	fraction
$Mmax_{MEZ}$	Maximum mortality mesozooplankton at 0°C	0.004	d ⁻¹
$Mmax_{MIZ}$	Maximum mortality microzooplankton at 0°C	0.030	d ⁻¹
KM_{MEZ}	Half-saturation mortality mesozooplankton	0.07	mmol-N m ⁻³
KM_{MIZ}	Half-saturation mortality microzooplankton	0.02	mmol-N m ⁻³
Ths_{MIZ}	Half-saturation temperature microzooplankton	4	°C
SVM_{MEZ}	Seasonal vertical migration mesozooplankton	0-25	m d ⁻¹
Detritus and nutrients			
DN	Mineralisation of detritus at 0°C	0.001	d ⁻¹
DN_{Si}	Mineralisation of Si-detritus at 0°C	0.0001	d ⁻¹

<i>NI₀</i>	Maximum nitrification rate at 0 °C	0.02	d ⁻¹
<i>K_{nit}</i>	Oxygen half-saturation in nitrification	3.75	mmol-O ₂ m ⁻³
<i>K_{denit}</i>	Nitrate half-saturation in denitrification	0.135	mmol-NO ₃ m ⁻³
<i>T_{sen}</i>	Temperature coefficient on recycling processes	0.07	°C ⁻¹
<i>SEDR</i>	Sinking rate detritus	-20	m d ⁻¹
RQN	Respiratory quotient in nitrification	2.0	O ₂ :NO ₃
RQC	Respiratory quotient in detritus	1.0	O ₂ :Organic-N
<i>S_{DET}</i>	Settling rate detritus	20	m d ⁻¹

960
961

962

963 **11.2 Appendix B, the ocean model (HYCOM)**

964 The ocean model (HYCOM) has 40 hybrid vertical levels, combining isopycnals with z-level
965 coordinates and sigma coordinates. Tides are included internally within the ocean model using
966 eight constituents and similar tides are added at the open boundaries using the Oregon State
967 University TOPEX/Poseidon Global Inverse Solution (TPXO 8.2,) Egbert and Erofeeva, 2002).
968 More than 100 rivers are included as monthly climatological discharges obtained from the
969 Global Runoff Data Centre (GRDC, <http://grdc.bafg.de>) and scaled as prescribed by Dai and
970 Trenberth (2002)(Dai and Trenberth, 2002). In addition the globally gridded Core v2 runoff data
971 (Large and Yeager, 2009) is added for Greenland, the Canadian Archipelago, Svalbard, and
972 islands within the Arctic Ocean.

973 The sea ice model (CICE) describes the dynamics and thermodynamics of the sea ice as
974 described by Rasmussen et al, 2018 (Rasmussen et al., 2018). The dynamics is driven by drag
975 from wind and ocean, surface tilt of the ocean, Coriolis force, and the internal strength of sea ice
976 that will resist movement of the ice pack. The internal strength is based on the Elastic-Viscous-
977 Plastic (EVP) sea-ice rheology (Hunke, 2001), that originates from the Viscous-Plastic (VP)
978 described by Hibler (1979)(Hibler, 1979). CICE includes 5 thickness categories of sea ice within
979 each grid cell in order to describe the inhomogeneity. The thermodynamics prescribes a vertical
980 temperature profile with a resolution of four sea ice layers and one layer of snow for each sea-ice
981 category (Bitz and Lipscomb, 1999). Snow is very important for the thermodynamics of sea ice
982 as it insulates sea ice from the atmosphere and has a higher albedo than sea ice. The lower
983 boundary is governed by the upper ocean temperature, which is usually the ocean freezing
984 temperature and is linearly dependent on its salinity. The upper boundary is governed by the heat
985 and radiation transfer between the atmosphere and the combined snow/ice surface. The net heat
986 flux is calculated based on the 2m atmospheric temperature, humidity, incoming long and short-
987 wave radiation, and 10m wind and the state of the surface of the sea-ice model.

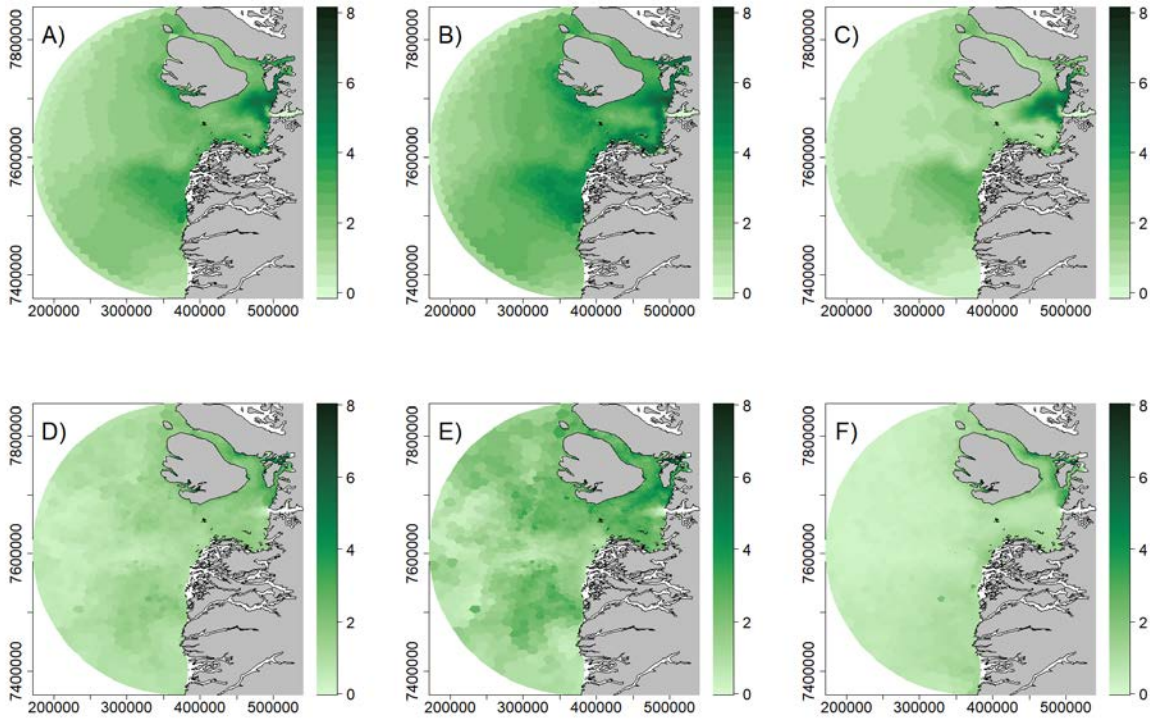
988 The HYCOM and CICE models used in this paper are coupled on each time step using the Earth
989 System modeling Framework (ESMF) coupler (Collins et al., 2004). The HYCOM-CICE set-up
990 at DMI used in this paper covers the Arctic Ocean and the Atlantic Ocean, north of about 20°S,
991 with a horizontal resolution of about 10 km (Madsen et al., 2016)..

992 The HYCOM-CICE model system assimilates re-analyzed sea-surface temperature
993 (<https://podaac.jpl.nasa.gov/GHRSST>, Høyer et al., 2012, 2014) and sea ice concentration
994 provided by the EUMETSAT Ocean and Sea Ice Satellite Application Facility (OSI SAF,
995 www.osi-saf.org, Lavergne et al., 2019) on a daily basis. The model is initialized in summer
996 1997 using the Polar Science Center Hydrographic Climatology (PHC; Steele et al., 2001) in the
997 Arctic Ocean and World Ocean Atlas 2001 0.25° (Conkright et al., 2002) in the Atlantic, with a
998 100 km linear transition. The atmospheric forcing is obtained from the Era-Interrim reanalysis
999 (Dee et al., 2011) until 2017 and thereafter deterministic HRES ECMWF forcing
1000 (www.ecmwf.int).

1001 **11.3 Appendix C, Figures**

1002

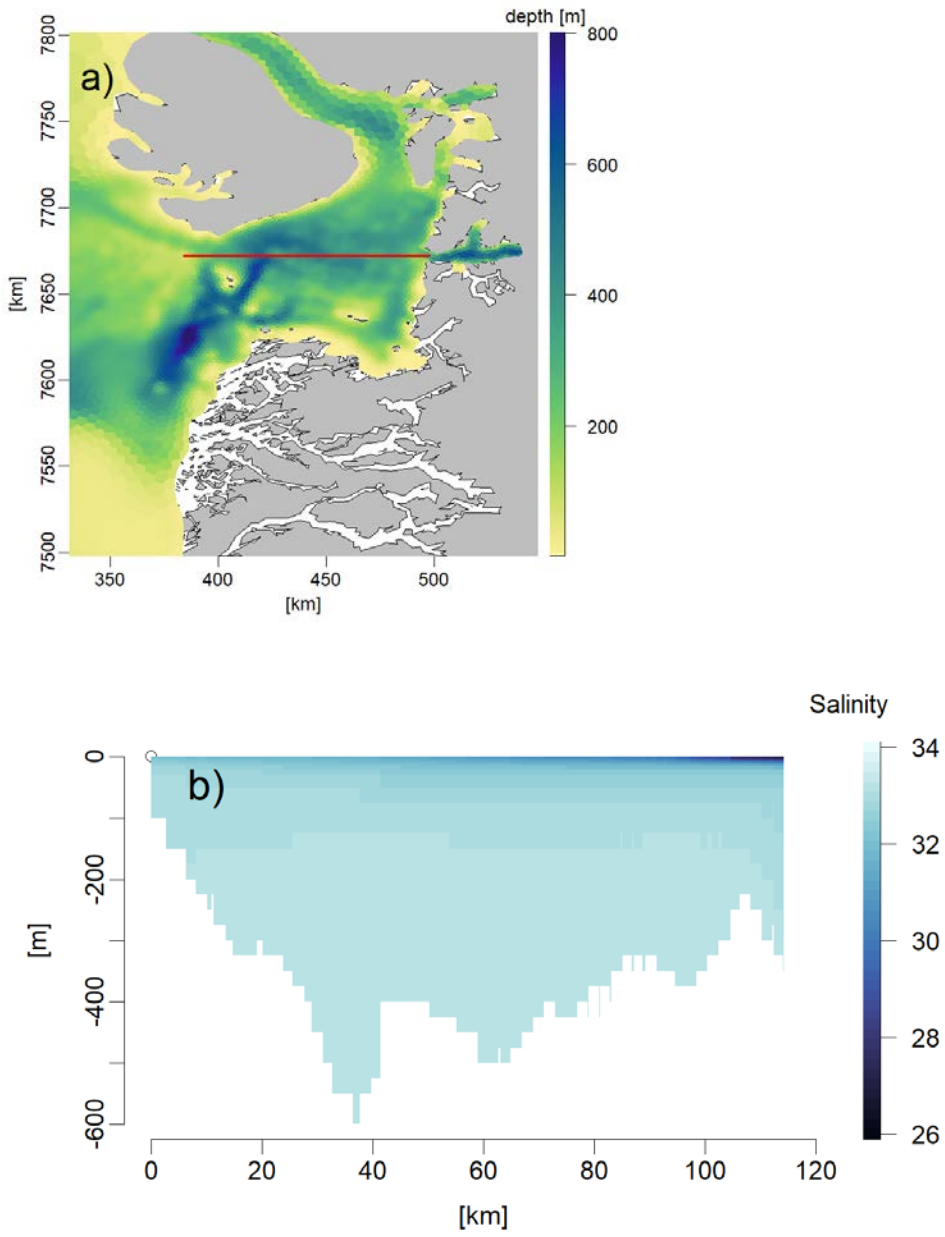
Figure C1: Surface Chl *a* concentration (mg chl *a* m⁻³) in 2010 obtained from the model (A-C) and from remote sensing (D-F). A) and D) are annual averages, B) and E) are April-June averages, and C) and F) are July-September averages.



1003

1004

Figure C2: a) Position and b) bathymetry of transect (x-axis: distance in km, y-axis: depth in m) shown in Figure C3.

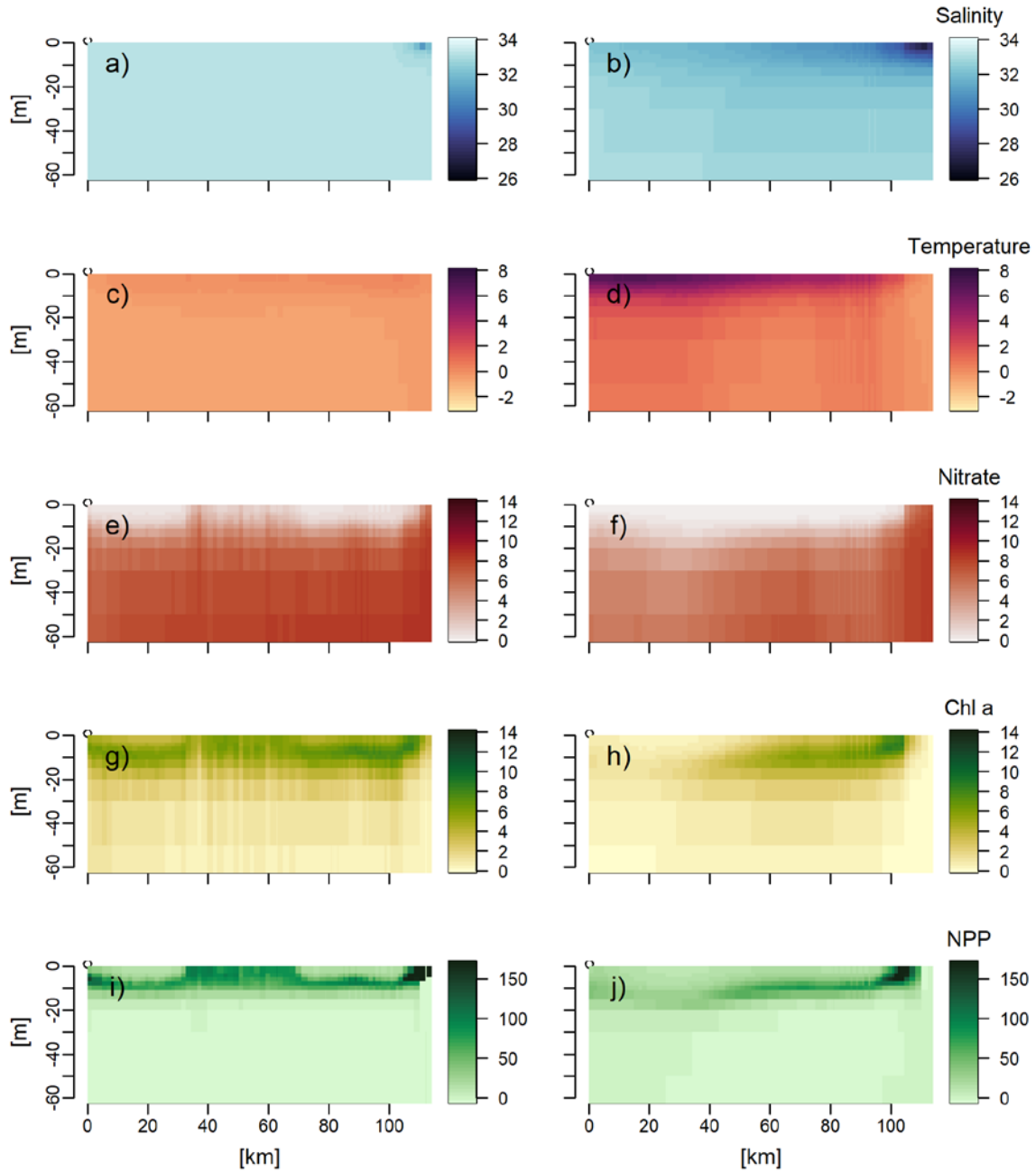


1005

1006

1007

Figure C3: Transects (x-axis: distance in km, y-axis: depth in m) of salinity (a, b) temperature ($^{\circ}\text{C}$) (c, d), DIN (mmol m^{-3}) (e, f), Chl *a* (mg m^{-3}) (g, h) and NPP ($\text{mgC m}^{-3} \text{d}^{-1}$) (i, j) in April (left) and August (right) 2010 along the transect shown in figure C2:



1008

1009

Figure C4. Vertical profiles of a) East-West velocities and b) vertical velocities at the ice edge in Jakobshavn Isbræ for 2010, the scenario noQNP, and the scenario with subglacial discharge at the glacier grounding line.

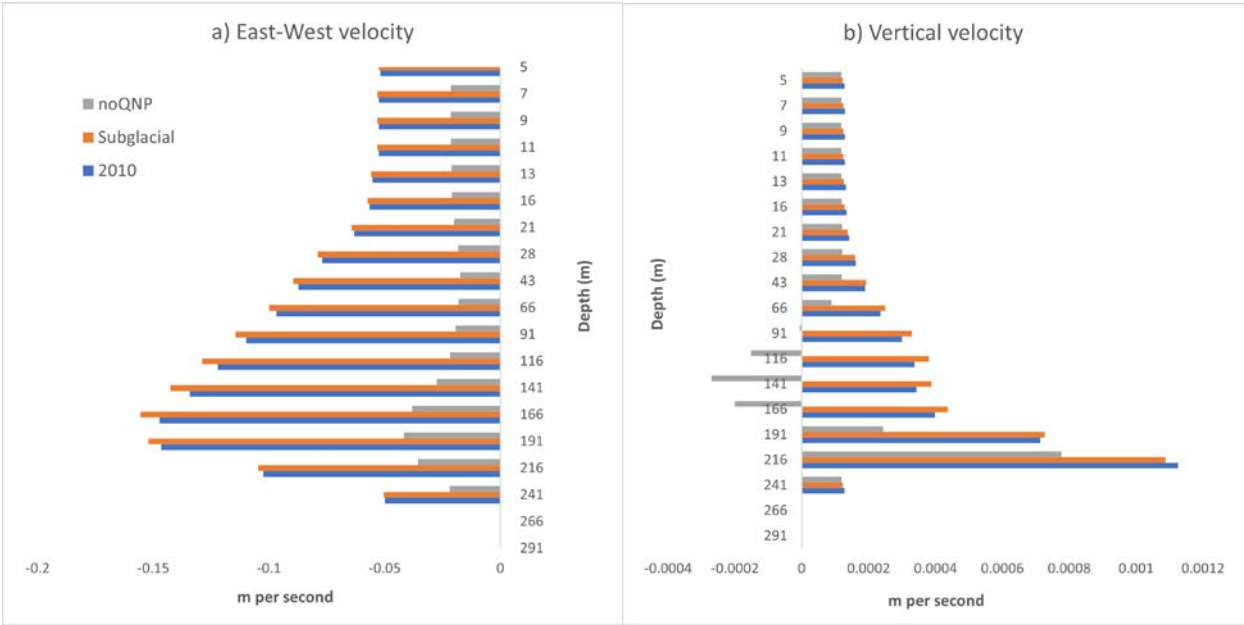
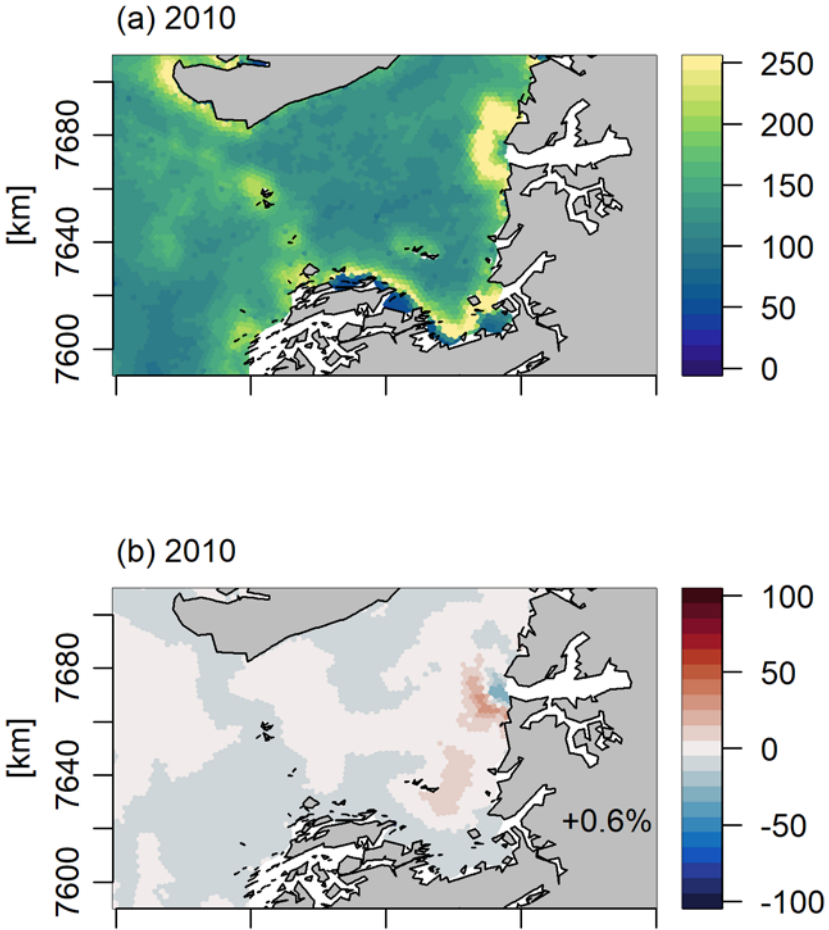


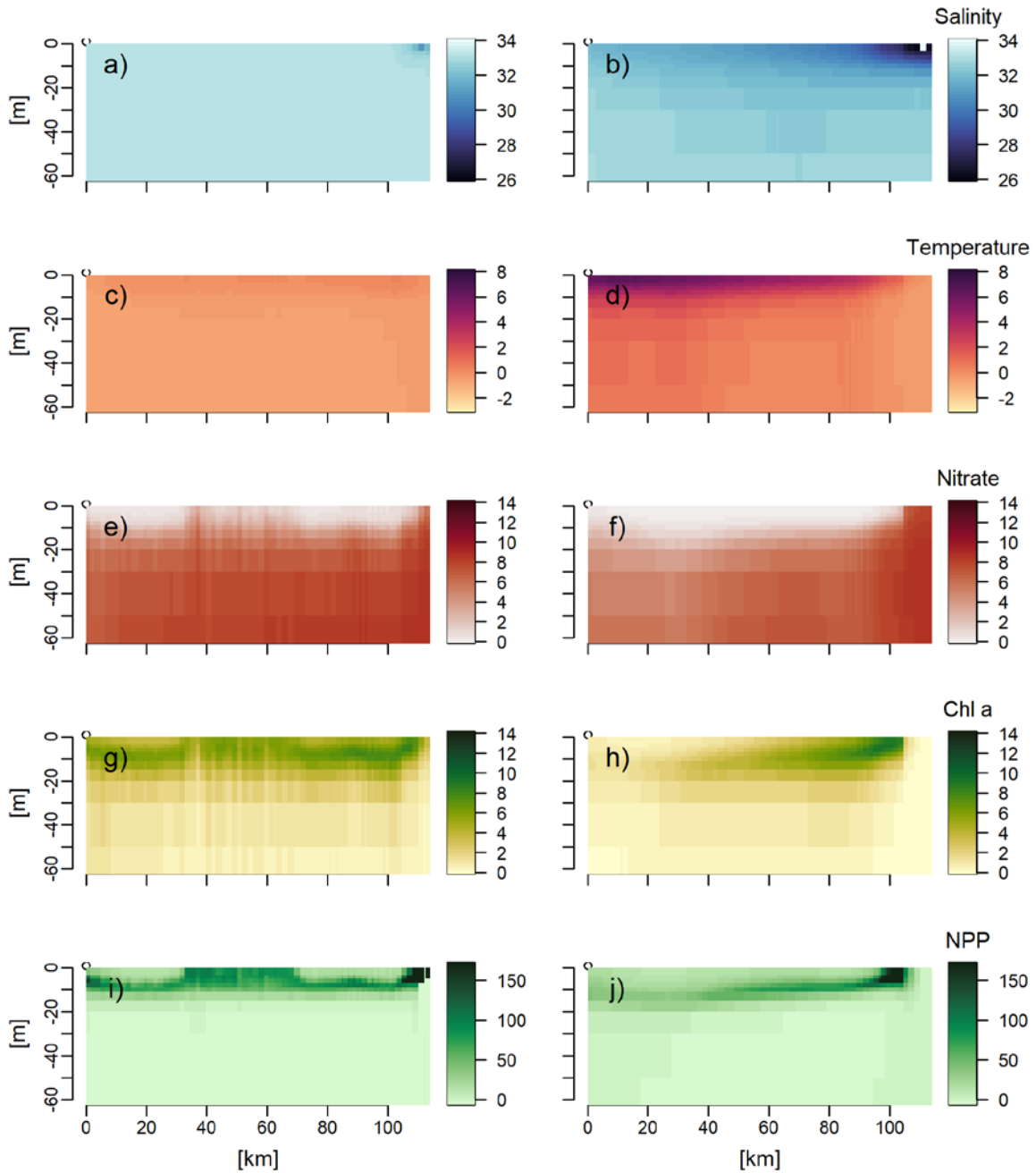
Figure C5: Annual primary production in 2010 (a) when the ice runoff is inserted at the glacier grounding line instead of in the surface as in the standard model run (Fig C3), and percentage change relative to the standard model run (b). The percentages in the bottom of the figure (b) are the changes in primary production in the total area shown.



1010

1011

Figure C6: Transects (x-axis: distance in km, y-axis: depth in m) of salinity (a, b) temperature (°C) (c, d), DIN (mmol m^{-3}) (e, f), Chl *a* (mg m^{-3}) (g, h) and NPP ($\text{mgC m}^{-3} \text{d}^{-1}$) (i, j) in April (left) and August (right) 2010 along the transect shown in figure C2 when the ice runoff is inserted at the glacier grounding line instead of in the surface as in the standard model run (Fig C3).



1012

1013

